Applied Numerical Mathematics 118 (2017) 87–116

Contents lists available at ScienceDirect

Applied Numerical Mathematics

www.elsevier.com/locate/apnum

High-order numerical solution of the Helmholtz equation for domains with reentrant corners ☆

S. Magura [a], S. Petropavlovsky [b,a], S. Tsynkov [a,c,*], E. Turkel [d]

[a] Department of Mathematics, North Carolina State University, Box 8205, Raleigh, NC 27695, USA
[b] National Research University Higher School of Economics, 20 Myasnitskaya Ulitsa, Moscow 101000, Russia
[c] Moscow Institute of Physics and Technology, Dolgoprudny, 141700, Russia
[d] School of Mathematical Sciences, Tel Aviv University, Ramat Aviv, Tel Aviv 69978, Israel

ARTICLE INFO

Article history:
Received 13 February 2017
Received in revised form 24 February 2017
Accepted 25 February 2017
Available online 2 March 2017

Keywords:
Singularity subtraction
Regularization
Asymptotic expansion near singularity
Difference potentials
Curvilinear boundaries
Compact differencing

ABSTRACT

Standard numerical methods often fail to solve the Helmholtz equation accurately near reentrant corners, since the solution may become singular. The singularity has an inhomogeneous contribution from the boundary data near the corner and a homogeneous contribution that is determined by boundary conditions far from the corner. We present a regularization algorithm that uses a combination of analytical and numerical tools to distinguish between these two contributions and ultimately subtract the singularity. We then employ the method of difference potentials to numerically solve the regularized problem with high-order accuracy over a domain with a curvilinear boundary. Our numerical experiments show that the regularization successfully restores the design rate of convergence.

1. Introduction

We consider a time-harmonic wave problem on a bounded 2D domain with a reentrant corner, as shown schematically in Fig. 1. Problems with reentrant corners are difficult because the solution may become singular near the corner, i.e., the derivatives of the solution become unbounded. Standard numerical methods perform poorly near singularities, so they must be modified before use on singular problems. Wave problems with reentrant corners may arise, for instance, when analyzing the scattering of radar waves near an air–ocean–sea ice interface [23]. Marin et al. have solved several Helmholtz-type equations on domains with reentrant corners in [29] and [28] with the boundary element method (BEM) and the method of fundamental solutions (MFS), respectively. Martinsson [30] has applied an efficient spectral method to the Helmholtz equation on an L-shaped domain, though the method cannot handle arbitrarily-shaped boundaries and there is no attempt to remove the singularity. A variety of techniques [2], such as the Method of Particular Solutions (MPS) [6,42], have been

☆ Work supported by the US Army Research Office (ARO) under grants # W911NF-11-1-0384 and # W911NF-16-1-0115, and by the United States–Israel Binational Science Foundation (BSF) under grant # 2014048.

* Corresponding author at: Department of Mathematics, North Carolina State University, Box 8205, Raleigh, NC 27695, USA.
E-mail addresses: srmagura@ncsu.edu (S. Magura), spetropavlovsky@gmail.com (S. Petropavlovsky), tsynkov@math.ncsu.edu (S. Tsynkov), turkel@post.tau.ac.il (E. Turkel).
URLs: http://www.math.ncsu.edu/~srmagura (S. Magura), http://www.math.ncsu.edu/~stsynkov (S. Tsynkov), http://www.math.tau.ac.il/~turkel/ (E. Turkel).

http://dx.doi.org/10.1016/j.apnum.2017.02.013
0168-9274/

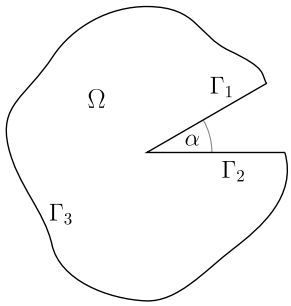

Fig. 1. A schematic for the domain Ω with a reentrant corner.

applied to the eigenvalue problem for the Laplacian on an L-shaped domain. Reentrant corners have been studied most thoroughly in the civil and mechanical engineering literature in the context of loaded elastic bodies, see [21] for a survey.

A somewhat different approach to the numerical treatment of near-boundary singularities does not tackle those singularities directly. It rather smoothes out the corners and replaces them with sharply bent yet smooth curves. Then, the solution near the "corners" is no longer singular; it formally remains regular although its derivatives are large and the sharper the boundary curve the larger the derivatives. This approach has been applied, in particular, in work [12] to computing the Laplace eigenvalues on an L-shaped domain similar to that studied in [6].

In this paper, we use regularization (also known as singularity subtraction) and the method of difference potentials [38] to achieve high-order accuracy near a corner. Singular solutions to the boundary value problem (BVP) that are expected to hamper numerical convergence are first subtracted out to produce a regularized problem, whose solution is known ahead of time to be smooth enough to be solved numerically without loss of accuracy. The regularized problem is then solved numerically with the method of difference potentials. Finally the solution to the original boundary value problem is obtained by adding the singular solutions back to the regular solution. Our algorithm computes the regularization with sufficient accuracy to restore the intended high-order convergence rate of the method of difference potentials. This is an improvement over previous works, e.g. by Marin et al. [29,28], that did not present data on the rate of convergence. High-order accuracy is particularly important for highly oscillatory wave propagation problems because it limits the pollution effect [5,3], so this is a significant advantage of our method. Regularization also performs better than the classical approach of local mesh refinement in the vicinity of the singularity, see e.g. [43], since the mesh must be refined very aggressively near the singularity to maintain high-order accuracy (which leads to a deterioration of conditioning).

The issue of regularization is difficult because there may be two contributions to the singularity which must be handled individually. If we temporarily ignore the boundary condition on the outer boundary Γ_3, we can write the solution u to the Helmholtz equation over the domain Ω as $u = v + w$, where v is a particular solution that satisfies the boundary conditions on the sides of the wedge and w is an arbitrary linear combination of solutions that satisfy the homogeneous boundary conditions. Both the particular solution v and the linear combination w may be singular. We refer to the singularity in v as the inhomogeneous contribution to the singularity, and the singularity in w as the homogeneous contribution to the singularity. The inhomogeneous contribution is local, in the sense that it is determined by the boundary conditions in the vicinity of the corner. On the other hand, the homogeneous contribution is nonlocal, since the unknown coefficients that characterize w are determined by the data at the outer boundary Γ_3. To compute these unknown coefficients for use in the regularization, we must know what portion of the boundary data on Γ_3 is from w, and what portion is from v. When both v and w are nonzero, "splitting" the data on Γ_3 becomes a challenging issue. In this way, our work is more general than that of Marin et al. [29,28], who considered problems with only homogeneous contributions to the singularity.

While we choose to solve the regularized problem using the method of difference potentials due to its versatility and high-order accuracy, we emphasize that the regularized problem can be solved using whatever method is deemed most appropriate, such as the finite element method (FEM), BEM, or a spectral element method. This flexibility in choosing the numerical method is enabled by the partition between the regularization and the numerical solution per se. It is a key advantage of our approach over strategies for addressing the singularity that are reliant on a specific numerical method, such as FEM with special elements [1].

The method of difference potentials [37,38,36,44,31,32,10,33], introduced by Ryaben'kii, uses discrete counterparts to Calderon's operators to accommodate general curvilinear boundaries while leveraging the accuracy and efficiency of high-order finite difference schemes. In this way, the method of difference potentials overcomes a primary limitation of finite difference methods, their inability to accurately handle boundaries that do not conform to the discretization grid. The method of difference potentials has the same asymptotic complexity as finite difference schemes on regular structure grids. In FEM, on the other hand, high-order accurate approximations can be built for arbitrarily shaped boundaries only in fairly sophisticated and costly algorithms with isoparametric elements, see e.g. [4, Chapter 4]. In discontinuous enrichment/discontinuous Galerkin methods and GFEM [16,22,17,46], high-order accuracy also requires additional degrees of freedom. The downside of these methods for the predominantly smooth problems (geometrically large regions with smooth material parameters separated by several interface boundaries) is their substantial redundancy, which entails an additional compu-

tational cost. Difference potentials also have several advantages over the methods based on classical integral equations, like BEM: singular integral kernels do not have to be evaluated, and variable coefficients (inhomogeneous media) and nonstandard boundary conditions can be handled naturally [31,10]. In our subsequent development, we combine the method of difference potentials with a fourth order accurate finite difference scheme on a compact 3×3 stencil [9]. Note that sixth order accurate schemes on the same compact stencil have also been constructed for both the constant coefficient Helmholtz equation [41] and variable coefficient Helmholtz equation [45]. Compact schemes are beneficial as they only need the boundary conditions of the original BVP — additional artificial boundary conditions are unnecessary.

In our earlier work [11], we have already used the method of difference potentials to compute singular solutions to the Helmholtz equation with high-order accuracy. In that paper, however, the singularity was due to a discontinuity in the boundary data, while the boundary itself remained smooth. As a result, there was no homogeneous contribution to the singularity (more precisely, the corresponding part of the expansion was regular), and the overall formulation proved easier to analyze. The authors of [25,24,26], on the other hand, apply the method of difference potentials for computing singular solutions caused by the geometry of the domain. Yet that work does not pursue the high-order accuracy. Another example of employing the method of difference potentials for computing solutions with singularities is the recent work [39], as well as [47,48], where the authors simulate fractures in linear elasticity with second order accuracy.

1.1. Formulation and basic analysis of the problem

We solve the Helmholtz equation, which governs the propagation of time-harmonic acoustic waves or electromagnetic waves without polarization. In particular, we consider the homogeneous Helmholtz equation with a constant wavenumber k,

$$\Delta u + k^2 u = 0.$$

The computational domain Ω, shown schematically in Fig. 1, has a reentrant corner at the origin. Let $\alpha > 0$ be the angle of the reentrant corner, measured exterior to the domain, and denote the segments of the boundary Γ by Γ_1, Γ_2, and Γ_3 as shown in the figure. The boundary value problem is formulated with Dirichlet boundary conditions on each piece of Γ,

$$\Delta u + k^2 u = 0 \quad \text{on } \Omega, \tag{1a}$$

$$u\big|_{\Gamma_1} = \varphi_1, \quad u\big|_{\Gamma_2} = \varphi_2, \quad u\big|_{\Gamma_3} = \varphi_3. \tag{1b}$$

We assume that the solution $u = u(r,\theta)$ of the BVP (1) exists and is unique, i.e., that $-k^2$ is not a Dirichlet eigenvalue of the Laplacian on Ω. If $-k^2$ proves to be such an eigenvalue, then problem (1) is said to have an interior resonance. We do not address this case, since the solution is not unique. However, even when $-k^2$ is near a resonance rather than exactly at a resonance, solving problem (1) may be problematic because the resulting discrete operator (a matrix) will be nearly singular and hence poorly conditioned. Therefore, in practice we must require that not only problem (1) be non-resonant, but also that $-k^2$ be sufficiently far away from all resonances.

Hereafter, we assume that the solution u to problem (1) is bounded, although we allow the derivatives of u to be unbounded near the corner. The Dirichlet boundary condition on Γ, defined piecewise by φ_1, φ_2, and φ_3, is assumed to guarantee that the solution u of the BVP (1) is sufficiently regular away from the corner. When φ_1 and φ_2 have unbounded derivatives near the corner, the solution u will be singular. Yet, we will show that there are also singular solutions equal to zero on both sides of the wedge.

We assume we know a function $v = v(r,\theta)$ that satisfies the Helmholtz equation (1a), as well as the boundary conditions on the sides of the wedge, but does not necessarily satisfy the boundary condition at the outer boundary:

$$\Delta v + k^2 v = 0, \tag{2a}$$

$$v\big|_{\Gamma_1} = \varphi_1, \quad v\big|_{\Gamma_2} = \varphi_2. \tag{2b}$$

The function v of (2) may also be singular at the origin, but does not necessarily coincide with the solution u of the boundary value problem (1). Consider the difference of the two functions:

$$w = u - v.$$

The function $w = w(r,\theta)$ is a solution of the following BVP:

$$\Delta w + k^2 w = 0 \quad \text{on } \Omega, \tag{3a}$$

$$w\big|_{\Gamma_1} = 0, \quad w\big|_{\Gamma_2} = 0 \tag{3b}$$

$$w\big|_{\Gamma_3} = \tilde{\varphi}_3 = \varphi_3 - v\big|_{\Gamma_3}. \tag{3c}$$

The general solution to equation (3a) subject to the homogeneous boundary conditions (3b) on the sides of the wedge can be sought for in the form of a series (obtained by separation of variables):

$$w(r,\theta) = \sum_{m=1}^{\infty} \hat{w}_m(r) \sin(m\nu(\theta - \alpha)), \quad \text{where} \quad \nu = \frac{\pi}{2\pi - \alpha}. \tag{4}$$

We adopt the convention that the coordinate θ is in the interval $[\alpha, 2\pi]$ for every point in the closure $\bar{\Omega}$, so that there is no ambiguity when evaluating the functions $\sin(m\nu(\theta-\alpha))$, which are not 2π-periodic. Due to the special choice of ν, each term of the series (4) satisfies zero Dirichlet boundary conditions on the sides of the wedge. We apply the Helmholtz operator to w to determine the Fourier coefficients $\hat{w}_m(r)$. We recall that in polar coordinates, the Laplacian is

$$\Delta = \frac{\partial^2}{\partial r^2} + \frac{1}{r}\frac{\partial}{\partial r} + \frac{1}{r^2}\frac{\partial^2}{\partial \theta^2}.$$

As the sine functions in (4) are orthogonal on the interval $\alpha \le \theta \le 2\pi$ for the different values of m, substitution of the series (4) into the Helmholtz equation (3a) yields the following ODE for each $\hat{w}_m(r)$, $m = 1, 2, \ldots$:

$$\frac{d^2\hat{w}_m}{dr^2} + \frac{1}{r}\frac{d\hat{w}_m}{dr} + k^2\hat{w}_m - \frac{m^2\nu^2}{r^2}\hat{w}_m = 0. \tag{5}$$

Denoting $kr = x$, we transform the previous equation into the Bessel equation for $\hat{w}_m$:

$$x^2\frac{d^2\hat{w}_m}{dx^2} + x\frac{d\hat{w}_m}{dx} + (x^2 - m^2\nu^2)\hat{w}_m = 0. \tag{6}$$

Equation (6) is a second-order ODE, so its general solution is a linear combination of two linearly independent solutions. Hence, $\hat{w}_m(x) = a_m J_{m\nu}(x) + b_m Y_{m\nu}(x)$, where $J_{m\nu}$ and $Y_{m\nu}$ are the Bessel functions of the first and second kind, respectively, with order $m\nu$. We require the solution u to be bounded. But, $Y_{m\nu}(x)$ is unbounded as $x \to 0^+$, so we have

$$\hat{w}_m = a_m J_{m\nu}(x) = a_m J_{m\nu}(kr).$$

Hence, the series (4) becomes:

$$w(r,\theta) = \sum_{m=1}^{\infty} a_m J_{m\nu}(kr)\sin(m\nu(\theta-\alpha)). \tag{7}$$

The coefficients a_m are referred to as "flux intensity factors" in [27,29,28], and are analogous to the "stress intensity factors" in elastostatics, see [21]. We will simply call them *intensity factors*. The intensity factors are currently unknown, but can be determined by enforcing the boundary condition (3c):

$$w\big|_{\Gamma_3} = \tilde{\varphi}_3 = \varphi_3 - v\big|_{\Gamma_3}.$$

If the angle α is acute, then $1/2 < \nu < 2/3$, for ν defined in (4). For $m = 1$ and small kr, we can write $J_\nu(kr) = \mathcal{O}((kr)^\nu)$, which means that though the Bessel function J_ν itself is bounded at the origin, its first derivative is already unbounded. For $m = 2$ we have $J_{2\nu}(kr) = \mathcal{O}((kr)^{2\nu})$, so the first derivative is bounded but the second derivative is unbounded. Subsequent terms of the series (7) will have increasing regularity at the origin. Here we assumed that α was acute only for illustrative purposes — the regularity of the terms improves with m for any $\alpha \in (0, 2\pi)$.

Altogether, we conclude that the singularity of the solution u to BVP (1) at the origin ($r = 0$) has an inhomogeneous contribution due to v of (2) and a homogeneous contribution due to w of (3). We write the inhomogeneous contribution as a log-power series using a method proposed by Fox and Sankar [18] in 1969, in which each term has increased regularity than the previous term. The homogeneous contribution comes from the terms of the Fourier–Bessel series (7), which also have increasing regularity. Our goal is to calculate several leading terms of the series for the homogeneous and inhomogeneous contributions. Then, subtracting these singular terms from the original BVP (1) for u will yield a problem that is smooth enough to be solved by difference potentials.

Computing the intensity factors $\{a_m\}$ via relation (3c) proves challenging for problems with nonzero boundary conditions on the sides of the wedge, because we need to know v to evaluate $\tilde{\varphi}_3$. The function v can be any solution of the homogeneous Helmholtz equation (2a) that satisfies the nonzero boundary conditions (2b) on the sides of the wedge. Because there is no boundary condition on the outer boundary, v is not unique; to see this, assume v satisfies the Helmholtz equation (2b) and boundary conditions (2b). But (2a) and (2b) will still be satisfied if any term $J_{m\nu}(kr)\sin(m\nu(\theta-\alpha))$ of the Fourier–Bessel series is added to v, since this Fourier–Bessel term is zero on the sides of the wedge.

We only need *some* function v satisfying (2). Hence, not only doesn't this lack of uniqueness hurt us, it can be used to our advantage (see Section 2). Additionally, v only needs to be evaluated on the outer boundary Γ_3, so it suffices to formulate and solve a boundary value problem for v on a larger intermediate domain that contains the curve Γ_3. We take the outer boundary of this intermediate domain to be an arc that encloses Γ_3 and employ a method based on separation of variables to define the boundary condition.

A specific question of central importance for any numerical method applied to the Helmholtz equation is how this method would scale with respect to the wavenumber k. For the method that we propose in the current paper, the answer to this question is two-fold. On one hand, our regularization algorithm employs a series representation of the solution and subtracts several leading singular terms of this series so that the remaining part of the solution becomes sufficiently smooth. For higher wavenumbers, such a series may converge slower, because the magnitude of its individual terms may increase as k increases, and hence more terms would be needed to reach a given threshold for the residual. However, the

conventional convergence of the series does not directly affect the performance. In fact, the series by Fox and Sankar [18] is, generally speaking, asymptotic, and its convergence is not guaranteed at all. What we actually require from the series used for regularization is not the convergence per se; it is rather the increasing regularity of its successive terms. As shown in Section 2.1, this property is not related to the value of k.

On the other hand, the regularized problem is already guaranteed to have a well-behaved solution, and is solved numerically. For that purpose, we use the method of difference potentials [38], which relies on a finite difference approximation. Moreover, whereas the number of leading singular terms in the regularizing expansion that one needs to use does not depend on k, the coefficients in front of those terms (referred to as the intensity factors, see equation (7)) are computed using an auxiliary numerical procedure that also involves finite differences (see Section 2.4). It is well-known that any finite difference approximation of the Helmholtz equation is prone to numerical pollution [5]. It means that the approximation error is proportional to the quantity $k^p h^{p+1}$, where h is the grid size and p is the order of accuracy. Thus, to maintain a fixed discretization error the number of points per wavelength kh must grow as $k^{1/p}$. For higher order schemes this growth is slower. Therefore, we use a fourth order accurate compact scheme [8] for computing the intensity factors and a similar scheme [40] in the core of our difference potentials algorithm. We also note that the pollution effect manifests itself for FEM the same way as it does for finite differences, see [3,15].

In Section 2, we describe our regularization method in full detail. In particular, Section 2.7 contains a concise step-by-step overview of the algorithm. Section 3 covers the method of difference potentials, with a focus on practical implementation rather than the underlying theory (see [31] for a recent account of difference potentials in combination with compact high order schemes for the Helmholtz equation). In Section 4, we present our numerical results. In Section 5, we summarize our findings and make suggestions for future work.

2. Regularization method

We begin the in-depth discussion of our regularization method by summarizing the results of Fox and Sankar [18], who derive a power series representation for the solution in a neighborhood of the corner. We then use this series as part of a procedure for defining and solving a boundary value problem for v. Once v is computed, we reduce the full problem (1) to a homogeneous problem (3) with zero boundary conditions on the sides of the wedge, and enforce boundary condition (3c) to calculate the leading intensity factors. Then, the final step is to subtract the homogeneous and inhomogeneous terms of the regularization from the full problem.

The goal is to create a regularized problem whose solution is "sufficiently smooth", i.e. smooth enough to restore the accuracy of the main numerical method near the corner. As such, the meaning of the term "sufficiently smooth" depends on which numerical method is used for the main solve. To keep our analysis general, we call a function sufficiently smooth/regular if the function and its first d derivatives are bounded in Ω. For the numerical experiments in Section 4, we found $d = 4$ to be sufficient for our fourth order difference potentials formulation.

2.1. The method of Fox and Sankar

The work [18] of Fox and Sankar enables one to remove the inhomogeneous contribution of the singularity and serves as a starting point for defining the boundary value problem for v. They describe a procedure for computing u in the form of an infinite series that contains pure power and log-power terms w.r.t. r (the powers may be fractional). The series can be expressed as

$$u(r,\theta) \sim \sum_{m=1}^{\infty} \left[v^{(m)}(r,\theta) + a_m w^{(m)}(r,\theta) \right], \tag{8}$$

where

$$\sum_{m=1}^{\infty} v^{(m)} = \sum_{m=1}^{\infty} r^{(m-1)+\eta} (A_m(\theta) \ln r + B_m(\theta)), \qquad \eta \geq 0, \tag{9}$$

is an asymptotic series for the function v that satisfies the Helmholtz equation (2a) and the Dirichlet boundary conditions on the sides of the wedge (2b). On the other hand, the series

$$\sum_{m=1}^{\infty} a_m w^{(m)} \tag{10}$$

is an arbitrary linear combination of functions $w^{(m)}$ that satisfy the homogeneous Helmholtz equation (3a) and homogeneous Dirichlet boundary conditions (3b) on the wedge.

Fox and Sankar's analysis provides a constructive procedure for determining the terms of the series (9) unambiguously from the Helmholtz equation (2a) and the boundary conditions (2b); in doing so, the next term in the series is explicitly computed based on the previous terms. So while v is not unique, the functions $\{v^{(m)}\}$ are. For the series (10), we take

$w^{(m)}(r,\theta) = J_{m\nu}(kr)\sin(m\nu(\theta-\alpha))$ since the Fourier–Bessel series (7) is the general solution to problem (3a)–(3b) that can be derived by separation of variables. Fox and Sankar propose to compute each function $w^{(m)}$ as a power series, similar to (9), instead of using separation of variables. This is done apparently because the methodology of [18] is more general and allows for the wavenumber k to vary. For our analysis and computations, we will rather use the genuine separation of variables and the Fourier–Bessel series (7). This approach only applies when k is constant, but it is more intuitive and straightforward to use.

The method of Fox and Sankar [18] is not equivalent to the true separation of variables, because the individual terms of the series (9) are not solutions to the homogeneous Helmholtz equation (2a). It is similar in the sense that each subsequent term of the series (9) is more regular than the previous term. The terms of the series $\sum_{m=1}^{\infty} v^{(m)}$ which are not sufficiently regular are what we refer to as the *inhomogeneous contribution* to the singularity. Similarly, the terms of the series $\sum_{m=1}^{\infty} a_m J_{m\nu}(kr)\sin(m\nu(\theta-\alpha))$ which are not sufficiently regular are referred to as the *homogeneous contribution* to the singularity. We remove both contributions of the singularity via the regularization

$$u = u^{(\mathrm{reg})} + v^{(1)} + \ldots + v^{(M_v)} + \sum_{m=1}^{M_w} a_m J_{m\nu}(kr)\sin(m\nu(\theta-\alpha)). \tag{11}$$

Here, the fixed integers M_v and M_w should be chosen large enough that the regularized solution $u^{(\mathrm{reg})} = u^{(\mathrm{reg})}(r,\theta)$ has d bounded derivatives at the corner. The first terms of the asymptotic series (8) that are not removed by the regularization (11) are $v^{(M_v+1)}$ and $w^{(M_w+1)}$:

$$v^{(M_v+1)}(r,\theta) = r^{(M_v)+\eta}(A_{M_v+1}(\theta)\ln r + B_{M_v+1}(\theta)),\ \eta \geq 0, \tag{12a}$$

$$w^{(M_w+1)}(r,\theta) = J_{(M_w+1)\nu}(kr)\sin((M_w+1)\nu(\theta-\alpha)). \tag{12b}$$

Thus if $M_v + \eta \geq d$, then $v^{(M_v+1)}$ has d bounded derivatives. For small values of kr we have $J_{m\nu}(kr) = \mathrm{const}\cdot(kr)^{m\nu} + o\big((kr)^{m\nu}\big)$, so $w^{(M_w+1)}$ has d bounded derivatives if and only if $(M_w+1)\nu \geq d$. In conclusion, $u^{(\mathrm{reg})}$ will be sufficiently regular when the constants M_v and M_w satisfy

$$M_v \geq d - \eta \quad \text{and} \quad M_w \geq \frac{d}{\nu} - 1. \tag{13}$$

For any $\alpha > 0$, we have $\nu > 1/2$, so $M_w = 2d-1$ will always be sufficient. The regularization (11) will eventually be used to convert the original boundary value problem (1) for u into a regularized boundary value problem for $u^{(\mathrm{reg})}$. Before doing that, the undetermined intensity factors $a_1, \ldots, a_{M_w}$ must be computed.

2.2. Splitting the inhomogeneous and homogeneous contributions to the singularity

The intensity factors are determined by the boundary conditions, yet they cannot be computed directly from the original boundary value problem (1), since the boundary data φ_3 on the outer boundary Γ_3 includes a contribution from v as well as from the Fourier–Bessel series (7). If we obtain v, then we can isolate the contribution to φ_3 that is due to the Fourier–Bessel series. The function v is required to satisfy the homogeneous Helmholtz equation (2a) and boundary conditions (2b), because this allows us to reduce the original boundary value problem (1) to a boundary value problem (3) with zero data on the sides of the wedge by considering $w = u - v$. Since the boundary value problem (3) for w has zero data on the sides of the wedge, its solution must be in the form of a Fourier–Bessel series (7). Then the leading M_w intensity factors may be determined by enforcing the boundary condition on w at Γ_3. Specifically, we require that the Fourier–Bessel series equals $\tilde{\varphi}_3 = \varphi_3 - v|_{\Gamma_3}$ on Γ_3, see (3c).

As mentioned previously, v is not unique because any term $J_{m\nu}(kr)\sin(m\nu(\theta-\alpha))$ of the Fourier–Bessel series can be added to v, and it will still satisfy the Helmholtz equation and boundary conditions (2b) on the sides of the wedge. Thus

$$\sum_{m=1}^{\infty} v^{(m)}(r,\theta) + \sum_{m=1}^{\infty} \tilde{a}_m J_{m\nu}(kr)\sin(m\nu(\theta-\alpha)) \tag{14}$$

is an asymptotic series for v for any choices of the coefficients $\{\tilde{a}_m\}$. Then,

$$\tilde{\varphi}_3 = \Big[(a_m - \tilde{a}_m) J_{m\nu}(kr)\sin(m\nu(\theta-\alpha))\Big]\Big|_{\Gamma_3}, \tag{15}$$

where the coefficients $\{a_m\}$ are the intensity factors of the original, full problem. Then equating the Fourier–Bessel series with $\tilde{\varphi}_3$ of (15) via boundary condition (3c) yields $\{a_m - \tilde{a}_m\}_{m\leq M_w}$ as the intensity factors. To recover the intensity factors $\{a_1, \ldots, a_{M_w}\}$ needed to regularize the original BVP (1), the numbers $\{\tilde{a}_1, \ldots, \tilde{a}_{M_w}\}$ must be known. Suppose we are able compute a v such that $\tilde{a}_1 = \cdots = \tilde{a}_{M_w} = 0$, i.e., a v that has the asymptotic series[1]

[1] Note that the difference between formulae (14) and (16) is in the summation range for the second sum.

$$\sum_{m=1}^{\infty} v^{(m)}(r,\theta) + \sum_{m=M_w+1}^{\infty} \tilde{a}_m J_{m\nu}(kr)\sin(m\nu(\theta-\alpha)) \tag{16}$$

for some choice of constants $\tilde{a}_{M_w+1}, \tilde{a}_{M_w+2}, \ldots$. Then enforcement of boundary condition (3c) will produce the desired intensity factors $a_1, \ldots, a_{M_w}$, since all the coefficients $\{\tilde{a}_m\}_{m\le M_w}$ are 0. The condition that v admits the asymptotic series (16) is equivalent to requiring that the singularity in v comes from the inhomogeneous contribution only. It makes intuitive sense that this condition is necessary to obtain the intensity factors, because the reason for partitioning u as $v+w$ is to separate the two contributions to the singularity.

We cannot compute v by summing the asymptotic series (16), since the series $\sum_{m=1}^{\infty} v^{(m)}$ from the method of Fox and Sankar [18] is not necessarily convergent. Instead, we first subtract the M_v singular terms from v so that the difference $\tilde{v} = v - v^{(1)} - \ldots - v^{(M_v)}$ satisfies [cf. problem (2)]

$$\Delta\tilde{v} + k^2\tilde{v} = f, \tag{17a}$$

$$\tilde{v}\big|_{\Gamma_1} = \tilde{\varphi}_1, \quad \tilde{v}\big|_{\Gamma_2} = \tilde{\varphi}_2. \tag{17b}$$

Note that, as the individual terms $v^{(m)}$ built according to Fox and Sankar [18] are not solutions to the homogeneous Helmholtz equation, equation (17a), unlike equation (2a), develops an inhomogeneity that we denote f:

$$f := -(\Delta + k^2\boldsymbol{I})\big(v^{(1)} + \ldots + v^{(M_v)}\big). \tag{18}$$

By design, the function f that is defined by (18) and appears on the right-hand side of equation (17a), is such that the solution $\tilde{v}$ is non-singular, i.e., has at least d bounded derivatives.

Moreover, subtracting only the leading terms $v^{(1)} + \ldots + v^{(M_v)}$ does not make the boundary conditions on the wedge (17b) homogeneous either, as we have:

$$\tilde{\varphi}_1 = \varphi_1 - \big(v^{(1)} + \ldots + v^{(M_v)}\big)\big|_{\Gamma_1},$$
$$\tilde{\varphi}_2 = \varphi_2 - \big(v^{(1)} + \ldots + v^{(M_v)}\big)\big|_{\Gamma_2}.$$

Neither $\tilde{\varphi}_1$ nor $\tilde{\varphi}_2$ is necessarily equal to zero on its respective domain (Γ_1 or Γ_2). Nevertheless, the inhomogeneity of the boundary conditions (17b) can be removed by an easy modification of both $\tilde{v}$ and f, which still keeps the solution non-singular at the tip of the wedge. We provide the details in Section 2.3. In the meantime, we recast problem (17) as

$$\Delta\tilde{v} + k^2\tilde{v} = \tilde{f}, \tag{19a}$$

$$\tilde{v}\big|_{\Gamma_1} = 0, \quad \tilde{v}\big|_{\Gamma_2} = 0. \tag{19b}$$

Any solution $\tilde{v}$ to problem (19) can be represented as the sum of a particular solution to the inhomogeneous equation and the general solution to the homogeneous equation:

$$\tilde{v} = \tilde{v}_{\mathrm{p}}(r,\theta) + \sum_{m=M_w+1}^{\infty} \tilde{a}_m J_{m\nu}(kr)\sin(m\nu(\theta-\alpha)). \tag{20}$$

While the coefficients $\tilde{a}_m$ on the right-hand side of (19) can be arbitrary, our key constraint is that the expansion for the general solution to the homogeneous equation should start from $m = M_w + 1$, i.e., as in (16). This will guarantee that the homogeneous contribution remains non-singular. As for the inhomogeneous contribution $\tilde{v}_{\mathrm{p}}(r,\theta)$, it is non-singular[2] by construction, because $\tilde{v}$ is obtained from v by subtracting the M_v leading singular terms according to Fox and Sankar.

We emphasize that problem (19) is not a proper BVP for the Helmholtz equation because it is not closed — there is no outer boundary condition. Accordingly, this problem has multiple solutions. To find a solution $\tilde{v}$ to problem (19) in the form (20), we first represent it as a Fourier sine series:

$$\tilde{v} = \sum_{m=1}^{\infty} \tilde{V}_m(r)\sin(m\nu(\theta-\alpha)). \tag{21}$$

Using separation of variables, one immediately sees that the radial functions $V_m(r)$ on the right-hand side of (21) satisfy the inhomogeneous ordinary differential equations [cf. equation (5)]:

$$\frac{d^2\tilde{V}_m}{dr^2} + \frac{1}{r}\frac{d\tilde{V}_m}{dr} + k^2\tilde{V}_m - \frac{m^2\nu^2}{r^2}\tilde{V}_m = \hat{\tilde{f}}_m, \tag{22}$$

where $\hat{\tilde{f}}_m = \hat{\tilde{f}}_m(r)$ are the sine Fourier coefficients of $\tilde{f}(r,\theta)$ from the right-hand side of (19a).

[2] Being non-singular is understood here in the sense of Section 2.1; see, in particular, equation (13).

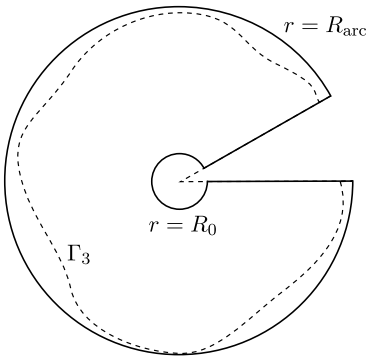

Fig. 2. A schematic for the intermediate domain Ω_{int} (solid lines) that contains Ω (dashed lines).

For our subsequent analysis, it will be convenient to split the sum (21) into two:

$$\tilde{v} = \underbrace{\sum_{m=1}^{M_w} \tilde{V}_m(r)\sin(m\nu(\theta-\alpha))}_{\tilde{v}_1} + \underbrace{\sum_{m=M_w+1}^{\infty} \tilde{V}_m(r)\sin(m\nu(\theta-\alpha))}_{\tilde{v}_2}. \tag{23}$$

The second sum on the right-hand side of (23) that we have denoted $\tilde{v}_2$ contains, in particular, the entire homogeneous contribution given by the Fourier–Bessel series on the right-hand side of (20).

To actually obtain $\tilde{v}_2 = \tilde{v}_2(r,\theta)$, we formulate a boundary value problem for each $\tilde{V}_m(r)$, i.e., for each differential equation (22), $m = M_w+1, M_w+2, \ldots$. To do so, we first notice that according to (12a), i.e., according to the regularity requirement for $\tilde{v}$, we have $\tilde{V}_m(0) = 0$. As for the outer boundary condition for $\tilde{V}_m(r)$, the existing flexibility in $\tilde{a}_m$ allows one to specify it at any sufficiently large $r = R_{\text{arc}}$ even though the true outer boundary Γ_3 is not an arc and does not allow the separation of variables. The value of R_{arc} should be chosen such that for every point (r,θ) on Γ_3 we have $r < R_{\text{arc}}$, see Fig. 2. Moreover, the key advantage of the split (23) is that for any $m \geq M_w+1$ the boundary condition for $\tilde{V}_m(r)$ at $r = R_{\text{arc}}$ can be arbitrary. Indeed, the non-singular behavior of $\tilde{v}_2$ is guaranteed ahead of time by the particular form of f, see formula (18), and the specific values of the coefficients $\tilde{a}_m$ in (20) do not matter. The simplest choice is to set $\tilde{V}_m(R_{\text{arc}}) = 0$ for $m = M_w+1, M_w+2, \ldots$. Then, we can say that $\tilde{v}_2$ delivers a bounded solution to the following boundary value problem [cf. problem (19)]:

$$\Delta\tilde{v}_2 + k^2\tilde{v}_2 = \tilde{f}_2, \tag{24a}$$

$$\tilde{v}_2\big|_{\Gamma_1} = 0, \quad \tilde{v}_2\big|_{\Gamma_2} = 0, \quad \tilde{v}_2\big|_{r=R_{\text{arc}}} = 0, \tag{24b}$$

where

$$\tilde{f}_2 := \sum_{m=M_w+1}^{\infty} \hat{\tilde{f}}_m(r)\sin(m\nu(\theta-\alpha)).$$

In doing so, we are assuming that $-k^2$ is not a Dirichlet eigenvalue of the Laplacian on the auxiliary domain bounded by the segments Γ_1, Γ_2 and the arc $r = R_{\text{arc}}$, see Fig. 2. In other words, we are assuming that $r = R_{\text{arc}}$ is not a root of any of the Bessel functions $J_{m\nu}(kr)$, $m = 1, 2, \ldots$. The latter requirement can be relaxed. It is sufficient that $J_{m\nu}(kR_{\text{arc}}) \neq 0$ only for $m = 1, 2, \ldots, M_w$, because the values of $\tilde{a}_m$ for $m \geq M_w+1$ in (20) can be arbitrary.

To obtain $\tilde{v}_1$ of (23), we need to solve the differential equations (22) for $m = 1, 2, \ldots, M_w$. Unlike in the case of $\tilde{v}_2$, however, the resulting solutions $\tilde{V}_m(r)$ may not contain any Bessel functions $J_{m\nu}(kr)$, since this would create a homogeneous contribution to singularity. Therefore, each equation (22), $m = 1, 2, \ldots, M_w$, shall be solved as an initial value problem (IVP). From (12a), we conclude that the initial conditions can be specified as

$$\tilde{V}_m(0) = 0, \quad \frac{d\tilde{V}_m(0)}{dr} = 0. \tag{25}$$

Solving IVPs (22), (25) for $m = 1, 2, \ldots, M_w$ on the interval $0 \leq r \leq R_{\text{arc}}$, we obtain a non-singular $\tilde{v}_1$ for (23), or, equivalently, a non-singular particular solution $\tilde{v}_{\text{p}}$ in (20). Moreover, as we only need to solve finitely many initial value problems (22), (25), and their number M_w remains fixed,[3] there is no potential for ill-posedness or discrete instability.

[3] M_w depends only on the desired degree of regularity, see (13), and does not depend on the parameters of the discretization that need to be chosen later.

2.3. The boundary value problem for v

In Section 2.2, we have shown how one can distinguish between the inhomogeneous and homogeneous contribution to singularity, which enabled a constructive approach to regularization for the original boundary value problem (1). In practice, the regularization described in Section 2.2, i.e., the functions $\tilde{v}_1$ and $\tilde{v}_2$ of (23), shall be computed. Therefore, in this section we introduce a somewhat different yet equivalent approach to building a regularization that proves more convenient for numerical implementation. We also provide the details that were omitted in the previous section.

In particular, we find it more efficient not to specify any boundary (or initial) conditions right at the corner. Instead, we will take a small step away from the corner and state a counterpart to BVP (24) over the intermediate domain shown in Fig. 2,

$$\Omega_{\text{int}} = \{(x, y) \in \mathbb{R}^2 : \alpha < \theta < 2\pi, \;\; R_0 < r < R_{\text{arc}}\},$$

where R_0 is small. Since the corner is not in Ω_{int}, the singularity does not disrupt the numerical convergence on Ω_{int}. Next, in Section 2.2 we considered the function $\tilde{v} = v - \left(v^{(1)} + \ldots + v^{(M_v)}\right)$, since subtracting the leading terms of the series of Fox and Sankar [18] eliminates the inhomogeneous contribution to the singularity. Now that the corner is outside Ω_{int}, we no longer need to subtract these terms ahead of time and can solve for the entire v rather than for $\tilde{v}$.

We now return to problem (2):

$$\Delta v + k^2 v = 0,$$
$$v\big|_{\Gamma_1} = \varphi_1, \quad v\big|_{\Gamma_2} = \varphi_2.$$

The functions $\varphi_1 = \varphi_1(r)$ and $\varphi_2 = \varphi_2(r)$ are defined for $0 \le r \le R$, since the radial segments Γ_1 and Γ_2 are assumed to be of length R. The auxiliary domain extends to the larger value of $r = R_{\text{arc}}$, so we create arbitrary smooth extensions of φ_1 and φ_2 to the larger set $[0, R_{\text{arc}}]$. Rather than introducing new notation, we simply redefine the symbols φ_1 and φ_2 to refer to their extensions. Any smooth extensions will work, since v only needs to satisfy the original boundary conditions (2b), which are stated for $0 \le r \le R$. We also show that convergence is restored for two distinct choices of the extension in our numerical experiments, see Section 4.

So far, we have the following conditions for v on the intermediate domain Ω_{int}:

$$\Delta v + k^2 v = 0 \qquad \text{on } \Omega_{\text{int}}, \tag{26a}$$
$$v\big|_{\theta=\alpha} = \varphi_1(r), \qquad R_0 \le r \le R_{\text{arc}}, \tag{26b}$$
$$v\big|_{\theta=2\pi} = \varphi_2(r), \qquad R_0 \le r \le R_{\text{arc}}. \tag{26c}$$

We now transform the incomplete BVP (26) so that it admits a Fourier sine series solution [cf. equation (21)]:

$$v = \sum_{m=1}^{\infty} V_m(r) \sin(m\nu(\theta - \alpha)). \tag{27}$$

For such a solution to exist, the Dirichlet boundary conditions on the sides of the wedge must be made homogeneous. To do this, we take an arbitrary smooth function $g = g(r, \theta)$ defined on Ω_{int} that matches the boundary conditions (26b), (26c):

$$g\big|_{\theta=\alpha} = \varphi_1(r),$$
$$g\big|_{\theta=2\pi} = \varphi_2(r), \qquad R_0 \le r \le R_{\text{arc}}.$$

Specifically, we take

$$g(r, \theta) = \frac{\theta - 2\pi}{\alpha - 2\pi}\varphi_1(r) + \frac{\theta - \alpha}{2\pi - \alpha}\varphi_2(r). \tag{28}$$

Then, rewriting the conditions (26) on v for the new function $v_g := v - g$, we obtain

$$\Delta v_g + k^2 v_g = -(\Delta + k^2 \boldsymbol{I})g =: f_g \qquad \text{on } \Omega_{\text{int}}, \tag{29a}$$
$$v_g\big|_{\theta=\alpha} = 0, \qquad R_0 \le r \le R_{\text{arc}}, \tag{29b}$$
$$v_g\big|_{\theta=2\pi} = 0, \qquad R_0 \le r \le R_{\text{arc}}. \tag{29c}$$

Subtracting g from v creates an equivalent problem with zero data on the sides of the wedge, at the cost of developing a nonzero right-hand side f_g. Now, we check if the functions $\{V_m\}$ in the sine series (27) can be chosen so that conditions (29) are satisfied. Applying the Helmholtz operator $(\Delta + k^2 \boldsymbol{I})$ to (27), we obtain:

$$\Delta v + k^2 v = \sum_{m=1}^{\infty} \left[\frac{d^2 V_m}{dr^2} + \frac{1}{r}\frac{dV_m}{dr} + \left(k^2 - \left(\frac{m\nu}{r}\right)^2\right) V_m \right] \sin(m\nu(\theta - \alpha)). \tag{30}$$

Hence, the series (27) can only satisfy Helmholtz equation (29a) if the right-hand side $f_g = -(\Delta + k^2 \boldsymbol{I})g$ is expressible as a Fourier sine series. Yet in general, the Fourier series of f_g may have nonzero cosine terms. Thus, we must modify (29) so that the right-hand side of the PDE is guaranteed to be 0 on the sides of the wedge.

To do this, we construct a smooth function q on Ω_{int} such that

$$\begin{aligned} q\big|_{\theta=\alpha} &= q\big|_{\theta=2\pi} = 0, \\ (\Delta + k^2\boldsymbol{I})q\,\big|_{\theta=\alpha} &= f_g(r,\alpha), \\ (\Delta + k^2\boldsymbol{I})q\,\big|_{\theta=2\pi} &= f_g(r,2\pi), \qquad\qquad 0 \le r \le R_{\text{arc}}. \end{aligned} \tag{31}$$

To break up this task, we define q as the sum $q_1 + q_2$, where the functions q_1 and q_2 are chosen so that

$$\begin{aligned} q_1\big|_{\theta=\alpha} &= q_1\big|_{\theta=2\pi} = 0, & q_2\big|_{\theta=\alpha} &= q_2\big|_{\theta=2\pi} = 0, \\ (\Delta + k^2\boldsymbol{I})q_1\big|_{\theta=\alpha} &= f_g(r,\alpha), & (\Delta + k^2\boldsymbol{I})q_2\big|_{\theta=\alpha} &= 0, \\ (\Delta + k^2\boldsymbol{I})q_1\big|_{\theta=2\pi} &= 0, & (\Delta + k^2\boldsymbol{I})q_2\big|_{\theta=2\pi} &= f_g(r,2\pi). \end{aligned}$$

We accomplish this by requiring that q_1, q_2, and their first and second radial derivatives are zero on the sides of the wedge. Then, the only contribution to $(\Delta + k^2\boldsymbol{I})q_1$ and $(\Delta + k^2\boldsymbol{I})q_2$ will come from the $\frac{1}{r^2}\frac{\partial^2}{\partial\theta^2}$ term of the Laplacian. In particular, one can take

$$\begin{aligned} q_1(r,\theta) &= r^2 \cdot \frac{1}{2}(\theta-\alpha)^2\, f_g(r,\alpha)\, P_2\left(\frac{\alpha-\theta}{2\pi-\alpha}+1\right), \\ q_2(r,\theta) &= r^2 \cdot \frac{1}{2}(\theta-2\pi)^2\, f_g(r,2\pi)\, P_2\left(\frac{\theta-2\pi}{2\pi-\alpha}+1\right), \end{aligned} \tag{32}$$

where $P_2(x) = 10x^3 - 15x^4 + 6x^5$ is a polynomial such that $P_2(0) = 0$ and $P_2(1) = 1$, with the first two derivatives equal to 0 at $x = 0, 1$. It can be verified directly that $q = q_1 + q_2$, with q_1 and q_2 as defined in (32), meets the requirements (31).

Then, substituting $v_{gq} := v_g - q$ into equations (29), we obtain:

$$\Delta v_{gq} + k^2 v_{gq} = f_g - (\Delta + k^2\boldsymbol{I})q =: f_{gq} \qquad \text{on } \Omega_{\text{int}}, \tag{33a}$$

$$v_{gq}\big|_{\theta=\alpha} = 0, \qquad R_0 \le r \le R_{\text{arc}}, \tag{33b}$$

$$v_{gq}\big|_{\theta=2\pi} = 0, \qquad R_0 \le r \le R_{\text{arc}}. \tag{33c}$$

The new right-hand side f_{gq} equals 0 when $\theta = \alpha$ or $\theta = 2\pi$, so f_{gq} can be written as a sine series at each r:

$$f_{gq}(r,\theta) = \sum_{m=1}^{\infty} \hat{f}_m(r)\sin(m\nu(\theta-\alpha)). \tag{34}$$

Then, setting

$$v_{gq}(r,\theta) = \sum_{m=1}^{\infty} V_m(r)\sin(m\nu(\theta-\alpha)), \tag{35}$$

separation of variables implies [cf. equation (22)]:

$$\frac{d^2V_m}{dr^2} + \frac{1}{r}\frac{dV_m}{dr} + \left(k^2 - \left(\frac{m\nu}{r}\right)^2\right)V_m = \hat{f}_m(r), \qquad R_0 < r < R_{\text{arc}},\ m = 1,2,\ldots. \tag{36}$$

We now split the series (35) for v_{gq}, as was done earlier in (23),

$$v_{gq} = \underbrace{\sum_{m=1}^{M_w} V_m(r)\sin(m\nu(\theta-\alpha))}_{v_1} + \underbrace{\sum_{m=M_w+1}^{\infty} V_m(r)\sin(m\nu(\theta-\alpha))}_{v_2}. \tag{37}$$

The Bessel functions $J_{m\nu}(kr)$ are sufficiently regular for $m \ge M_w + 1$, so the boundary condition on v_2 at the outer arc may be chosen arbitrarily. For simplicity, we take [cf. the last equation of (24b)]:

$$v_2\big|_{r=R_{\text{arc}}} = 0, \quad \alpha \le \theta \le 2\pi. \tag{38}$$

Section 2.2 suggests calculating $\tilde{v}_1$ by solving M_w ODE initial value problems (22), (25), and calculating $\tilde{v}_2$ by solving a PDE boundary value problem (24). Yet directly applying this strategy to v_1 and v_2 of (37) could make it challenging to recover the entire v_{gq} from the differing discretizations of v_1 and v_2. Instead, it will be more convenient to formulate and

numerically solve a single BVP for the entire v_{gq}. To do so, however, we need to have an outer boundary condition for v_1 and to obtain that, in turn, we will still solve M_w auxiliary IVPs for the ODEs (36).

Recall that the outer boundary condition for v_1 must be chosen precisely so as to not introduce a homogeneous contribution to the singularity. Suppose we supplement the ODEs (36) with appropriate initial conditions and numerically integrate to obtain approximations $V_m^*(R_{\text{arc}})$ of the function V_m at the outermost point $r = R_{\text{arc}}$. Then we can formulate the boundary condition

$$v_1\big|_{r=R_{\text{arc}}} = \sum_{m=1}^{M_w} V_m^*(R_{\text{arc}}) \sin(m\nu(\theta-\alpha)), \quad \alpha \le \theta \le 2\pi. \tag{39}$$

Adding together boundary conditions (38) and (39), we obtain a boundary condition for v_{gq} itself:

$$v_{gq}\big|_{r=R_{\text{arc}}} = \sum_{m=1}^{M_w} V_m^*(R_{\text{arc}}) \sin(m\nu(\theta-\alpha)), \qquad \alpha \le \theta \le 2\pi. \tag{40}$$

Now that we have constructed a boundary condition at the outer arc $r = R_{\text{arc}}$, only the boundary condition on the inner arc $r = R_0$ of the intermediate domain Ω_{int} is missing.

The asymptotic series (16) provides an accurate approximation of v in the neighborhood of the corner and can thus provide this last boundary condition. Namely, for a given number of terms M_I we have:

$$v(r,\theta) - \sum_{m=1}^{M_I} v^{(m)}(r,\theta) = \mathcal{O}(v^{(M_I+1)}) = \mathcal{O}(r^{M_I}), \quad \text{as } r \to 0.$$

Thus we can formulate the approximate boundary condition for v at the inner arc of the intermediate domain:

$$v\big|_{r=R_0} = \sum_{m=1}^{M_I} v^{(m)}(R_0,\theta), \qquad \alpha \le \theta \le 2\pi. \tag{41}$$

This boundary condition can be transformed into a boundary condition for v_{gq} by subtracting $(g+q)$ on the right-hand side of (41). The error of approximation in boundary condition (41) is $\mathcal{O}(R_0{}^{M_I})$, so the radius R_0 and number of terms M_I should be chosen so that this error is smaller than the expected accuracy of the overall method. Our choice of M_I is discussed in Section 4.

It only remains to derive the appropriate initial conditions for the ODEs (36), $m = 1, \dots, M_w$, at $r = R_0$ that would replace initial conditions (25) from Section 2.2. These initial conditions and the resulting boundary condition (39) for v_1 should guarantee that there will be no homogeneous contribution to the singularity. In that regard, we recall that initial conditions (25) were derived based on the expression (12a) for the leading term of $\tilde{v}$ upon removing the inhomogeneous contribution to singularity following Fox and Sankar [18]. Unlike in Section 2.2, in this section we use the full v rather than $\tilde{v}$. Therefore, the initial conditions for the ODEs (36), $m = 1, \dots, M_w$, should be derived from the boundary condition (41) at the inner arc $r = R_0$ and the analogous relation for the derivative $\frac{\partial v}{\partial r}$. The functions $\{V_m\}$ are the Fourier coefficients of $v_{gq} = v - g - q$, so we transform (41) by subtracting g and q, and taking the Fourier transform. Accordingly, consider the Fourier coefficients $\{S_m^{(0)}\}$ and $\{S_m^{(1)}\}$ such that

$$\sum_{m=1}^{\infty} S_m^{(0)} \sin(m\nu(\theta-\alpha)) = \left[\sum_{m=1}^{M_I} v^{(m)} - (g+q)\right]\Bigg|_{(R_0,\theta)} \tag{42a}$$

$$\sum_{m=1}^{\infty} S_m^{(1)} \sin(m\nu(\theta-\alpha)) = \left[\sum_{m=1}^{M_I} \frac{\partial v^{(m)}}{\partial r} - \frac{\partial}{\partial r}(g+q)\right]\Bigg|_{(R_0,\theta)}. \tag{42b}$$

Then, the set of initial value problems to be solved for obtaining (39) is [cf. IVPs (22), (25)]

$$\frac{d^2V_m}{dr^2} + \frac{1}{r}\frac{dV_m}{dr} + \left(k^2 - \left(\frac{m\nu}{r}\right)^2\right) V_m = \hat{f}_m(r), \quad R_0 < r < R_{\text{arc}}, \tag{43a}$$

$$V_m(R_0) = S_m^{(0)}, \qquad \frac{dV_m}{dr}\bigg|_{r=R_0} = S_m^{(1)}, \qquad m = 1, \dots, M_w. \tag{43b}$$

The IVPs (43) define the previously undetermined Fourier coefficients $V_1(r), \dots, V_{M_w}(r)$. Each of the M_w initial value problems (43) has its coefficients and the right-hand side smooth and bounded for $R_0 \le r \le R_{\text{arc}}$, and thus can be solved by a wide variety of standard numerical ODE integrators to obtain the quantities $V_m^*(R_{\text{arc}})$, $m = 1, \dots, M_w$.

Bringing together (33), (40), and (41), we obtain a fully-specified BVP for v_{gq}:

$$\Delta v_{gq} + k^2 v_{gq} = f_{gq} \qquad \text{on } \Omega_{\text{int}}, \tag{44a}$$

$$v_{gq}\big|_{\theta=\alpha} = 0, \qquad R_0 \le r \le R_{\text{arc}}, \tag{44b}$$

$$v_{gq}\big|_{\theta=2\pi} = 0, \qquad R_0 \le r \le R_{\text{arc}}, \tag{44c}$$

$$v_{gq}\big|_{r=R_0} = \sum_{m=1}^{M_I} v^{(m)}(R_0,\theta) - (g+q)\big|_{(R_0,\theta)}, \quad \alpha \le \theta \le 2\pi, \tag{44d}$$

$$v_{gq}\big|_{r=R_{\text{arc}}} = \sum_{m=1}^{M_w} V_m^*(R_{\text{arc}}) \sin(m\nu(\theta-\alpha)), \qquad \alpha \le \theta \le 2\pi. \tag{44e}$$

Following the framework established in Section 2.2, we transformed the problem (2) for v so that it would have a Fourier series solution. We then used the method of separation of variables to obtain a sequence of IVPs (43), which, when solved, provide a boundary condition for v_{gq} at the outer arc.

2.4. Numerical computation of v

This section covers the practical numerical solution of the sequence of independent IVPs (43) and the BVP (44) from the previous section. In particular, we discuss the computational cost of solving the IVPs and introduce a compact finite difference scheme for the BVP.

When numerically integrating the IVPs (43), the primary cost comes from evaluating the right-hand side $\hat{f}_m(r)$, defined in (34) as the m-th Fourier sine coefficient of f_{gq}. We evaluate $\hat{f}_m$ by performing a Discrete Sine Transform (DST) on f_{gq} at each r-value considered. The DST of a real sequence can be thought of as one half of a full discrete Fourier transform (DFT) applied to the sequence twice the length, which is obtained by reflecting the original sequence anti-symmetrically about an endpoint. We are able to use the DST because it is known ahead of time that f_{gq} equals zero at the endpoints $\theta = \alpha$, $\theta = 2\pi$ and hence only has sine functions in its Fourier series. Likewise, the coefficients $S_m^{(0)}$ and $S_m^{(1)}$ that specify the initial conditions are calculated by performing the DST on the right-hand sides of (42a) and (42b) respectively.

For a given $r = \tilde{r}$, the n-point DST returns the first n coefficients $\hat{f}_1(\tilde{r}), \hat{f}_2(\tilde{r}), \ldots, \hat{f}_n(\tilde{r})$. Then, since $n \ge M_w$ for any reasonable choice of n, a single DST yields the value of the right-hand side at $r = \tilde{r}$ for all of the initial value problems (43), $m = 1, \ldots, M_w$. Therefore, using the same grid $r_0, r_1, \ldots, r_n$ for each of the initial value problems may lower the computational cost, by allowing a single DST to be "shared" among the different IVPs. There is a trade-off, however, since a grid that is near-optimal for one IVP may be suboptimal for the others. If one chooses to use an explicit method, we expect linear multistep methods (e.g., Adams–Bashforth) to have a lower computational cost than Runge–Kutta methods, because multistep methods reuse evaluations of the right-hand side from previous steps.

Once the quantities $V_m^*(R_{\text{arc}})$ are obtained from the numerical solutions of the IVPs (43), the BVP (44) for v_{gq} can be formed. Its numerical solution, however, does not have to be based on separation of variables. Accordingly, it is no longer necessary to continue including the contributions of g and q into the BVP. Instead, we can recast the BVP (44) in terms of $v = v_{gq} + g + q$:

$$\Delta v + k^2 v = 0 \qquad \text{on } \Omega_{\text{int}}, \tag{45a}$$

$$v\big|_{\theta=\alpha} = \varphi_1, \qquad R_0 \le r \le R_{\text{arc}}, \tag{45b}$$

$$v\big|_{\theta=2\pi} = \varphi_2, \qquad R_0 \le r \le R_{\text{arc}}, \tag{45c}$$

$$v\big|_{r=R_0} = \sum_{m=1}^{M_I} v^{(m)}(R_0,\theta), \qquad \alpha \le \theta \le 2\pi, \tag{45d}$$

$$v\big|_{r=R_{\text{arc}}} = \sum_{m=1}^{M_w} V_m^*(R_{\text{arc}}) \sin(m\nu(\theta-\alpha)) + (g+q)\big|_{(R_{\text{arc}},\theta)}, \quad \alpha \le \theta \le 2\pi. \tag{45e}$$

Now we solve the boundary value problem (45) numerically.

As the intermediate domain Ω_{int} is a polar rectangle, problem (45) is easy to approximate using finite differences. Moreover, Ω_{int} does not include the reentrant corner, so the singularity in v is outside the computational domain. We define a polar grid, uniform in each direction:

$$\{(r_m, \theta_l) : r_m = R_0 + mh_r,\ \theta_l = \alpha + lh_\theta\},$$
$$h_r = \frac{R_{\text{arc}} - R_0}{N},\ m = 0, \ldots, N,\ h_\theta = \frac{2\pi - \alpha}{N},\ l = 0, \ldots, N. \tag{46}$$

We represent the solution v on the grid as $v_{m,l} = v(r_m, \theta_l)$. We employ the fourth order accurate scheme for Helmholtz equation in polar coordinates from our earlier work [8]. Since the Helmholtz equation (45) is homogeneous, all terms of the scheme that involve the right-hand side and its partial derivatives vanish. Thus, the scheme is

$$
\begin{aligned}
&\frac{1}{r_m}\frac{1}{h_r}\left(r_{m+1/2}\frac{v_{m+1,l}-v_{m,l}}{h_r} - r_{m-1/2}\frac{v_{m,l}-v_{m-1,l}}{h_r}\right)\\
&+\frac{1}{r_m^2}\frac{v_{m,l+1}-2v_{m,l}+v_{m,l-1}}{h_\theta^2}\\
&-\frac{h_r^2}{12}\left[-k^2\frac{v_{m+1,l}-2v_{m,l}+v_{m-1,l}}{h_r^2}\right]\\
&+\frac{1}{12h_\theta^2}\left[\frac{1}{r_{m+1}^2}\left(v_{m+1,l+1}-2v_{m+1,l}+v_{m+1,l-1}\right)\right.\\
&-\frac{2}{r_m^2}\left(v_{m,l+1}-2v_{m,l}+v_{m,l-1}\right)\\
&\left.+\frac{1}{r_{m-1}^2}\left(v_{m-1,l+1}-2v_{m-1,l}+v_{m-1,l-1}\right)\right]\\
&-\frac{h_r^2}{12r_m}\left[-k^2\frac{v_{m+1,l}-v_{m-1,l}}{2h_r}\right.\\
&-\frac{1}{2h_rh_\theta^2}\left(\frac{1}{r_{m+1}^2}\left(v_{m+1,l+1}-2v_{m+1,l}+v_{m+1,l-1}\right)\right.\\
&\left.\left.-\frac{1}{r_{m-1}^2}\left(v_{m-1,l+1}-2v_{m-1,l}+v_{m-1,l-1}\right)\right)\right]\\
&-\frac{h_r^2}{12r_m^2}\left(-k^2v_{m,l}-\frac{1}{r_m^2h_\theta^2}\left(v_{m,l+1}-2v_{m,l}+v_{m,l-1}\right)\right)\\
&+\frac{h_r}{12r_m^3}\left(v_{m+1,l}-v_{m-1,l}\right)\\
&+\frac{h_\theta^2}{12}\left[k^2\frac{v_{m,l+1}-2v_{m,l}+v_{m,l-1}}{h_\theta^2}\right]\\
&+\frac{1}{12h_r^2r_m}\left[r_{m+1/2}(v_{m+1,l+1}-v_{m,l+1}) - r_{m-1/2}(v_{m,l+1}-v_{m-1,l+1})\right.\\
&-2\left(r_{m+1/2}(v_{m+1,l}-v_{m,l}) - r_{m-1/2}(v_{m,l}-v_{m-1,l})\right)\\
&\left.+r_{m+1/2}(v_{m+1,l-1}-v_{m,l-1}) - r_{m-1/2}(v_{m,l-1}-v_{m-1,l-1})\right]\\
&+k^2v_{m,l}=0.
\end{aligned}
\tag{47}
$$

The discretization of the partial differential equation is supplemented with the discrete analogs of the Dirichlet boundary conditions (45b)–(45e),

$$v_{m,0} = \varphi_1(r_m), \tag{48a}$$

$$v_{m,N} = \varphi_2(r_m), \qquad m = 0, \ldots, N, \tag{48b}$$

$$v_{0,l} = \sum_{m=1}^{M_l} v^{(m)}(R_0, \theta_l), \tag{48c}$$

$$v_{N,l} = \sum_{m=1}^{M_w} V_m^*(R_{\text{arc}})\sin(m\nu(\theta_l-\alpha)) + (g+q)\big|_{(R_{\text{arc}},\theta_l)}, \qquad l = 1, \ldots, N-1. \tag{48d}$$

Note that discretization (48) of the Dirichlet boundary conditions (45b)–(45e) is straightforward and does not require any special steps for achieving high-order accuracy. Together, the scheme (47) and discrete boundary conditions (48) define a

linear system with $(N+1)^2$ equations and $(N+1)^2$ unknowns. The matrix of this system is sparse, and we use a standard direct solver for sparse linear systems to compute the solution.[4]

Now that we know v on the polar grid (46), we use interpolation to approximate v on the curvilinear boundary Γ_3, since this is necessary to form the function $\tilde{\varphi}_3 = \varphi_3 - v|_{\Gamma_3}$, see equation (3c). The polar grid is uniform and forms a rectangle with respect to the coordinates (r, θ), so high-order interpolation is possible. We use two-dimensional quintic spline interpolation, which has sixth order accuracy. Alternatively, the more widely used cubic splines, which are fourth order accurate, should still be enough to guarantee that the overall method is fourth order.

2.5. Calculation of intensity factors

The leading intensity factors $a_1, \ldots, a_{M_w}$ which characterize the homogeneous contribution to singularity are unknown at this point. These intensity factors must be computed so that the homogeneous contribution can be removed as a part of the regularization. The overall strategy for calculating the intensity factors is to 1) obtain a function v that satisfies (2) and (16) through the methodology of Sections 2.2, 2.3, and 2.4, 2) form the data $\tilde{\varphi}_3 = \varphi_3 - v|_{\Gamma_3}$, and 3) enforce boundary condition (3c). To enable this analysis, we assume that the outer boundary Γ_3 can be parameterized as

$$\Gamma_3 = \{(x, y) \equiv (r\cos\theta, r\sin\theta) \in \mathbb{R}^2 : \alpha \le \theta \le 2\pi,\ \ r = r_3(\theta)\} \tag{49}$$

in terms of the smooth single-valued[5] function $r_3(\theta)$. Clearly, r_3 should be such that $r_3(\alpha) = R = r_3(2\pi)$ so that Γ_3 connects with the radial segments Γ_1, Γ_2 of length R. Furthermore, we characterize the deviation of Γ_3 from the true arc of radius R by the quantity

$$\beta := \max_{\alpha \le \theta \le 2\pi} |r_3(\theta) - R|\,. \tag{50}$$

An important part of our analysis requires that the value of β be sufficiently small, see Section 2.5.1. The boundary data on Γ_3 can also be expressed as a function of the polar angle, $\varphi_3 = \varphi_3(\theta)$, so that boundary condition (3c) becomes

$$\sum_{m=1}^{\infty} a_m J_{m\nu}(kr)\sin(m\nu(\theta - \alpha)) = \tilde{\varphi}_3(\theta), \qquad \alpha \le \theta \le 2\pi\,. \tag{51}$$

We calculate the leading intensity factors by discretizing this boundary condition.

The next steps are to define a discretization grid on the perturbed boundary, and sample the Fourier–Bessel functions and $\tilde{\varphi}_3$ on the grid. Using the notation of Section 2.1, let $w^{(m)}$ denote the m-th term of the Fourier–Bessel series (7),

$$w^{(m)}(r, \theta) = J_{m\nu}(kr)\sin(m\nu(\theta - \alpha)).$$

Then, let $\overline{w}^{(m)}$ denote the restriction of $w^{(m)}$ to Γ_3, parameterized by θ, that is, $\overline{w}^{(m)}(\theta) = w^{(m)}(r_3(\theta), \theta)$, $\alpha \le \theta \le 2\pi$. The N_W-node discretization grid on Γ_3 is defined by $\theta_i = i \cdot \frac{2\pi - \alpha}{N_W + 1}$ for $i = 1, \ldots, N_W$. The infinite series in boundary condition (51) needs to be truncated before implementation on the computer, so we take the first M_a terms, where $M_w \le M_a < N_W$. For each $m = 1, \ldots, M_a$, we define a vector whose entries are the trace of the m-th Fourier–Bessel term on the grid:

$$w_m^0 := [\overline{w}_m(\theta_i)]_{i=1}^{N_W} = [J_{m\nu}(kr_3(\theta_i))\sin(m\nu(\theta_i - \alpha))]_{i=1}^{N_W}, \quad m = 1, \ldots, M_a. \tag{52}$$

Let W^0 be an $N_W \times M_a$ matrix that has the vectors $\{w_m^0\}$ as its columns, and let p be the trace of φ_3 on the grid: $p = [\varphi_3(r_3(\theta_i), \theta_i)]_{i=1}^{N_W}$. The overdetermined linear system $W^0\boldsymbol{a} = p$ should have an "almost classical" solution when M_a and N_W are sufficiently large, because the Fourier coefficients $\{a_m\}$ decay to 0 as m increases. We solve this system in the sense of least squares. Then the first M terms of $\boldsymbol{a}$ will be approximations of the required coefficients $a_1, \ldots, a_{M_w}$.

However, there is a difficulty, since the Bessel $J_{m\nu}(kr)$ decays very rapidly as m increases. For example, $J_{50}(2.3) \sim 10^{-62}$. So as m increases from 1 to M_a, the entries in the columns w_m^0 become extremely small. As a result, W^0 will be rank-deficient in the numerical sense for large M_a. Fortunately, there is a simple way to remedy this problem by redefining the columns. As long as β of (50) is sufficiently small, $J_{m\nu}(kR)$ will be near $J_{m\nu}(kr_3(\theta))$ for any $\theta \in [\alpha, 2\pi]$. Let $(w_m^0)_l$ denote the l-th entry of the column w_m^0. Then for any l we expect

$$\left|\frac{(w_m^0)_l}{J_{m\nu}(kR)}\right| = \left|\frac{J_{m\nu}(kr_3(\theta_l))}{J_{m\nu}(kR)}\right| \,|\sin(m\nu(\theta_l - \alpha))|$$

to about the same order of magnitude as $|\sin(m\nu(\theta - \alpha))|$. Here, we assume that R is such that $J_{m\nu}(kR) \neq 0$ for any $m = 1, 2, \ldots, M_a$. Thus, the problem of excessively small entries in the matrix can be resolved by redefining the columns: $w_m = w_m^0 / J_{m\nu}(kR)$ for $m = M_w + 1, \ldots, M_a$. The idea is that, by dividing these "small" columns by a number that is "similarly small", we bring the entries of the columns back to "reasonable" numbers. The first M_w columns as left the same,

[4] In work [8] where scheme (47) was first built, we used an FFT based solver in a setting periodic in θ.

[5] A region of $\mathbb{R}^2$ bounded by the curve that can be parameterized by means of a single-valued function $r = r(\theta)$, $0 \le \theta \le 2\pi$, is called star-shaped.

$w_m = w_m^0$, $m = 1, \ldots, M_w$, since the problem only arises as m becomes large. Let W denote the matrix with the modified columns, $W = [w_m]_{m=1}^{M_a}$. Then the linear system

$$W\boldsymbol{a} = p \tag{53}$$

is to be solved in the sense of least squares. Since the first M_a columns of the matrix were not modified, the first M_a terms of $\boldsymbol{a}$ will still yield approximations to $a_1, \ldots, a_{M_w}$.

We should emphasize, however, that even though the matrix W of system (53) has been modified so that no columns are excessively small, one may still wonder if W is necessarily full rank. This question is addressed in Section 2.5.1.

2.5.1. Proof of linear independence

The system (53) must have a unique least squares solution if the solution vector $\boldsymbol{a}$ is to yield reliable estimates of $a_1, \ldots, a_{M_w}$. Thus W must be full rank. When Γ_3 is a true arc, the columns of W are orthogonal, and hence W is full rank and there is a unique least squares solution. In the case of a perturbed boundary, we will prove that finite sets of the functions $\{\overline{w}^{(m)}\}$ defined by (52) are linearly independent when the quantity β of (50) is sufficiently small. Then, the columns $\{w_m\}$ will be linearly independent as well, provided that the grid on Γ_3 is sufficiently fine. Thus, W will be full rank and there will be a unique least squares solution. The proof utilizes the theory of singular values for linear operators, a generalization of singular values for matrices.

Definition 1. Let A be a compact linear operator on a separable Hilbert space. Then the eigenvalues of the operator $B = (A^*A)^{1/2}$ are called the *singular values*, or *s-numbers*, of A. We enumerate them in decreasing order, taking the multiplicities into account:

$$s_j(A) = \lambda_j(B), \quad j = 1, \ldots, \operatorname{rank}(B).$$

If $\operatorname{rank}(B) < \infty$, then we define $s_j(A) = 0$ for all $j > \operatorname{rank}(B)$.

Definition 1 can be found in [19, p. 26].[6] The reason we have introduced the singular values of compact operators is because the singular values tell us how much the operator would need to be perturbed to reduce its rank.

Theorem 1 *(Allahverdiev). If A is a compact operator on a separable Hilbert space, then for each $n \in \mathbb{N}$,*

$$s_n(A) = \inf\{\|A - \mathcal{L}\| : \mathcal{L} \text{ is an operator with rank} < n\},$$

where the norm is the operator norm induced by the norm of the Hilbert space.

Theorem 1, which appears in [19, p. 28], is the key result in our proof of linear independence. Theorem 1 refers to operators, while we wish to show the linear independence of a set of functions. We bridge the gap by creating an operator T_0 that has range $\operatorname{span}\{J_{m\nu}(kR)\sin(m\nu(\theta-\alpha))\}_{m=1}^n$, for some n. The sine functions are orthogonal, hence T_0 has rank n. Then we create a similar operator T that has range $\operatorname{span}\{\overline{w}^{(m)}\}_{m=1}^n = \operatorname{span}\{J_{m\nu}(kr_3(\theta))\sin(m\nu(\theta-\alpha))\}_{m=1}^n$. By reducing the value of β of (50), we can make $J_{m\nu}(kr_3(\theta))$ close to $J_{m\nu}(kR)$, which will make the norm $\|T - T_0\|$ small. Thus, Theorem 1 will imply that both operators have rank n.

Proposition 1. *Assume $J_{m\nu}(kR) \neq 0$ for any $m = 1, \ldots, n$. Then $\exists \delta > 0$ such that if $\beta < \delta$, then the functions $\{\overline{w}^{(m)}\}_{m=1}^n$ form a linearly independent set.*

Proof. For each $m \leq n$, let $b_m : [\alpha, 2\pi] \to \mathbb{R}$ be defined by $b_m(\theta) = \sin(m\nu(\theta-\alpha))$, and let $v_m = J_{m\nu}(kR)b_m$. Let $T_0 : L^2[\alpha, 2\pi] \to L^2[\alpha, 2\pi]$ be defined by

$$T_0\varphi = \sum_{m=1}^{n} \langle \varphi, v_m \rangle v_m,$$

where $\langle \cdot, \cdot \rangle$ is the $L^2[\alpha, 2\pi]$ inner product. T_0 is linear and bounded. The range of the operator is $\mathcal{R}(T_0) = \operatorname{span}\{b_m\}_{m=1}^n$, so $\operatorname{rank}(T_0) = \dim \mathcal{R}(T_0) = n$. The operator T_0 has finite rank and is therefore a compact operator. Let $s_1(T_0), s_2(T_0), \ldots$ be the singular values of T_0. Theorem 1 implies that $s_n(T_0) > 0$, since T_0 has rank n.

Let $\varepsilon \in \mathbb{R}$ be such that

$$0 < \varepsilon < \frac{s_n(T_0)}{\sum_{m=1}^n \|v_m\|_{L^2} \cdot \|b_m\|_{L^2}}. \tag{54}$$

[6] Monograph [19] states this definition and Theorem 1 for completely continuous operators. On a Hilbert space, an operator is completely continuous iff it is compact [14, p. 173]. We will use the more modern term, compact.

For each $m \le n$, the Bessel function $J_{m\nu}$ is continuous at $r = R$, so $\exists \delta_m > 0$ such that $|r - R| < \delta_m \Rightarrow |J_{m\nu}(kr) - J_{m\nu}(kR)| < \varepsilon$. Let $\delta = \min\{\delta_1, \dots, \delta_n\}$ and assume $\beta < \delta$.

Define another operator T on $L^2[\alpha, 2\pi]$ by

$$T\varphi = \sum_{m=1}^{n} \langle \varphi, v_m \rangle \overline{w}^{(m)}.$$

We want to use Theorem 1 to show that $\operatorname{rank}(T) = n$, so we estimate the operator norm of $T - T_0$. Assume $\|\varphi\|_{L^2} = 1$. Then

$$\|(T - T_0)\varphi\|_{L^2} = \left\| \sum_{m=1}^{n} \langle \varphi, v_m \rangle (\overline{w}^{(m)} - v_m) \right\|_{L^2} \tag{55a}$$

$$\le \sum_{m=1}^{n} |\langle \varphi, v_m \rangle| \cdot \|(J_{m\nu}(kr_3(\theta)) - J_{m\nu}(kR))b_m\|_{L^2} \tag{55b}$$

$$\le \sum_{m=1}^{n} \|\varphi\|_{L^2} \|v_m\|_{L^2} \varepsilon \|b_m\|_{L^2} \tag{55c}$$

$$= \varepsilon \sum_{m=1}^{n} \|v_m\|_{L^2} \|b_m\|_{L^2} < s_n(T_0), \tag{55d}$$

where (55c) holds by Cauchy–Schwarz and since $|r_3(\theta) - R| \le \beta < \delta \le \delta_m$. In (55d), the final inequality follows from the assumption on ε, see formula (54). Hence $\|T - T_0\| < s_n(T_0) = \inf\{\|T_0 - \mathcal{L}\| : \mathcal{L} \text{ is an operator with rank} < n\}$. As such, T may not have rank smaller than n, so $\operatorname{rank}(T) \ge n$. The range of T is $\operatorname{span}\{\overline{w}^{(m)}\}_{m=1}^{n}$, so $\{\overline{w}^{(m)}\}_{m=1}^{n}$ is a linearly independent set. □

The columns w_m of the matrix W are obtained by sampling the functions $\{\overline{w}^{(m)}\}_{m=1}^{M_a}$ on the discretization grid $\theta_1, \dots, \theta_{N_W}$ on the perturbed boundary. For $m > M_w$, the column is also multiplied by a constant. Assume that β is less than the δ supplied by Proposition 1 in the case $n = M_a$. Then $\{\overline{w}^{(m)}\}_{m=1}^{M_a}$ is a linearly independent set, so the columns $\{w_m\}_{m=1}^{M_a}$ are linearly independent as well, provided the number of samples N_W is large enough. Hence the matrix W is full rank, and the overdetermined linear system (53) has a unique least squares solution.

While one can use Proposition 1 to show that W is full rank, the proposition's claim should not be exaggerated. Proposition 1 does *not* imply that the countably infinite set $\{\overline{w}^{(m)}\}_{m=1}^{\infty}$ is linearly independent. Recall that an infinite set is linearly independent iff any finite subset is linearly independent. The proof of Proposition 1 shows that, for any finite subset $\{\overline{w}^{(m_j)}\}_{j=1}^{n}$ of the countably infinite set, we can always choose β small enough to make the subset linearly independent. But this choice of β may depend on the indices $m_1, \dots, m_n$. We have not shown the existence of a single $\beta > 0$ that works for any finite subset of $\{\overline{w}^{(m)}\}_{m=1}^{\infty}$.

2.6. The regularized problem

Standard numerical methods for PDEs including the method of difference potentials may lose convergence when the solution is singular. We remedy this issue by converting the original boundary value problem (1) to a regularized problem whose solution is known to have enough bounded derivatives to restore the rate of convergence. In Section 2.1, we proposed the regularization (11):

$$u = u^{(\mathrm{reg})} + v^{(1)} + \ldots + v^{(M_v)} + \sum_{m=1}^{M_w} a_m J_{m\nu}(kr) \sin(m\nu(\theta - \alpha))$$

and showed that $u^{(\mathrm{reg})}$ is sufficiently smooth when M_v and M_w are chosen large enough to satisfy inequalities (13). Now that we have identified a method for obtaining the leading intensity factors $a_1, \dots, a_{M_w}$, see Section 2.5, the regularization (11) can be used in practical computation.

Before reformulating the original BVP (1) in terms of $u^{(\mathrm{reg})}$, we modify the regularization slightly. The term $v^{(m)}$ is of the form $r^{(m-1)+\eta}(A_m(\theta) \ln r + B_m(\theta))$, $\eta \ge 0$, which will become large as r increases for higher values of m. This is undesirable, because the sum $v^{(1)} + \ldots + v^{(M_v)}$ may become many times larger than the solution $u^{(\mathrm{reg})}$. The terms $v^{(m)}$ are included in the regularization to remove the singularity at the corner $r = 0$, and therefore their behavior only matters in the vicinity of the corner. Thus, modifying the regularization at points away from the corner will not impact its effectiveness. We modify the regularization (11) so that the terms $v^{(1)}, \dots, v^{(M_v)}$ are gradually tapered off as r increases. Consider the function

$$P_6(x) = \begin{cases} 0, & x < 0 \\ x^7(924x^6 - 6006x^5 + 16380x^4 - 24024x^3 + 20020x^2 - 9009x + 1716), & 0 \le x \le 1 \\ 1, & x > 1 \end{cases}$$

from [11]. The piecewise polynomial function P_6 smoothly transitions from 0 to 1 over the interval $[0, 1]$. Its first six derivatives are continuous, while there is a jump in the seventh derivative. This discontinuity is inconsequential when the required degree of regularity d is ≤ 6. If greater regularity is required, i.e. $d > 6$, then a piecewise polynomial of higher degree can be used in place of P_6. Then, the tapered asymptotic expansion of v is

$$v^{(\text{asym})} = \left[v^{(1)} + \ldots + v^{(M_v)}\right] \cdot P_6\left(1 - \frac{r - R_0}{R - R_0}\right).$$

The factor $P_6\left(1 - \frac{r-R_0}{R-R_0}\right)$ equals 1 when $r < R_0$ with a smooth transition to 0 over the interval $[R_0, R]$. The choice of endpoints $[R_0, R]$ is mostly arbitrary, though an overly abrupt transition should be avoided. When $r < R_0$, $v^{(\text{asym})}$ is equal to the original sum of $v^{(1)} + \ldots + v^{(M_v)}$, so the new regularization

$$u = u^{(\text{reg})} + v^{(\text{asym})} + \sum_{m=1}^{M_w} a_m J_{m\nu}(kr)\sin(m\nu(\theta - \alpha)), \tag{56}$$

will still guarantee that $u^{(\text{reg})}$ is sufficiently regular.

As discussed in Section 2.1, the individual terms $v^{(1)}, v^{(2)}, \ldots$ are not solutions to the homogeneous Helmholtz equation, since the method of Fox and Sankar [18] is not equivalent to a true separation of variables. Therefore, $u^{(\text{reg})}$ satisfies an inhomogeneous Helmholtz equation. The inhomogeneity is obtained by applying the Helmholtz operator $\Delta + k^2\boldsymbol{I}$ to regularization (56) [cf. formula (18)]:

$$f := -(\Delta + k^2\boldsymbol{I})v^{(\text{asym})}.$$

Since $u^{(\text{reg})}$ is known to have d bounded partial derivatives w.r.t. r at the corner, it follows that f has $d-2$ bounded radial derivatives. The regularized boundary value problem is then

$$\Delta u^{(\text{reg})} + k^2 u^{(\text{reg})} = f \qquad \text{on } \Omega, \tag{57a}$$

$$u^{(\text{reg})}\big|_{\Gamma_1} = \varphi_1 - v^{(\text{asym})}\Big|_{\Gamma_1}, \qquad u^{(\text{reg})}\big|_{\Gamma_2} = \varphi_2 - v^{(\text{asym})}\Big|_{\Gamma_2}, \tag{57b}$$

$$u^{(\text{reg})}\big|_{\Gamma_3} = \varphi_3 - v^{(\text{asym})}\Big|_{\Gamma_3} - \sum_{m=1}^{M_w} a_m J_{m\nu}(kr_3(\theta))\sin(m\nu(\theta - \alpha)). \tag{57c}$$

The regularized problem (57) is solved by the method of difference potentials, which is described in Section 3.

Let us note that smoothing out the corners (the approach employed, e.g., in [12]) can also be thought of as a special form of regularization. It has the advantage of not requiring any expansions of the solution. However, its justification is more heuristic than rigorous. It assumes that the better the smooth curve approximates the actual corner, the closer the resulting solution will be to the actual singular solution. While intuitively this assumption holds, its justification may prove challenging. Moreover, in practical computations, if two different smooth curves approximate one and the same corner, then the resulting solutions will, generally speaking, be different as well.

Our regularization technique, on the other hand, is geared toward true corners with no smoothing. Even though the geometries that originate from real-life applications are often characterized by rounded corners, true corners provide a good model that is free from any ambiguities associated with the choice of smoothing. The advantage of our model is that it lends itself to rigorous analysis. Specifically, it enables accurate explicit subtraction of the singularity in the form of a truncated series, which is something we do not expect would be possible in the case of smoothed corners.

2.7. Summary of the algorithm

This section provides a high-level step-by-step summary of the regularization algorithm.

1. Set the required degree of regularity d and find values of M_v and M_w that satisfy (13). For the fourth order accurate difference potentials formulation described in this paper, see Section 3, $d = 4$ is sufficient. The value may differ depending on the type of the main numerical solver and the order of accuracy.
2. Follow the algorithm of Fox and Sankar [18] to obtain the terms $v^{(1)}, \ldots, v^{(M_I)}$. The integer M_I should be chosen large enough so that $S_m^{(0)}$, $S_m^{(1)}$ are computed with sufficient accuracy, see (42). For example, we chose $M_I = 10$.
3. Use the functions g and q defined in (28) and (32), respectively, to arrive at the initial value problems (43). Then numerically solve the IVPs (43) for $m = 1, \ldots, M_w$ to obtain the corresponding quantities $V_m^*(R_{\text{arc}})$.
4. Numerically solve the boundary value problem (45) over the intermediate domain Ω_{int} with the fourth order finite difference scheme (47), (48) for the Helmholtz equation in polar coordinates. The result is a solution $\{v_{m,l}\}$ on the grid (46).

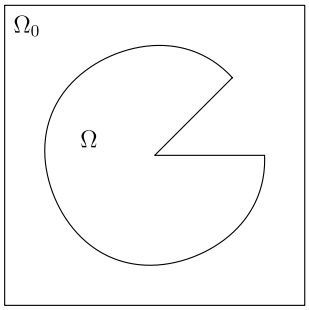

Fig. 3. The domain Ω is embedded in a rectangular auxiliary domain Ω_0.

5. Solve the linear system $W\boldsymbol{a} = p$, see (53), in the sense of least squares. In the computation of the vector p, a bivariate quintic spline interpolation of the discrete solution $\{v_{m,l}\}$ from the previous step should be used to evaluate $v|_{\Gamma_3}$. The first M_w entries of $\boldsymbol{a}$ are the required intensity factors $a_1, \ldots, a_{M_w}$.
6. Numerically solve the regularized problem (57). We choose to use the method of difference potentials for that purpose, see Section 3. However, our regularization algorithm is in no way specific to difference potentials. Other methods, such as FEM, can be used as well.

In the special case when Γ_3 is a true arc, the foregoing procedure becomes considerably simpler. Since the outer boundary is already a true arc, it makes sense to set $R_{\text{arc}} = R$, so that the outer boundary of the intermediate domain coincides with Γ_3. Then step 4 and the interpolation in step 5 become unnecessary since we do not need to know v on the interior of Ω_{int}. With the radius $r_3(\theta)$ constant along Γ_3, the boundary condition (51) becomes

$$\sum_{m=1}^{\infty} a_m J_{m\nu}(kR)\sin(m\nu(\theta-\alpha)) = \tilde{\varphi}_3, \quad \alpha \le \theta \le 2\pi,$$

which implies that the numbers $\{a_m J_{m\nu}(kR)\}$ are the Fourier sine coefficients of $\tilde{\varphi}_3$. Hence, the intensity factors $a_1, \ldots, a_{M_w}$ can be calculated by applying the DST to $\tilde{\varphi}_3$ and dividing by the constants $J_{m\nu}(kR)$. The system $W\boldsymbol{a} = p$ can still be used, but it may be simpler from an implementation perspective to use the DST.

3. The method of difference potentials

The method of finite differences suffers a loss of accuracy for problems whose boundaries do not conform to the discretization grid. The method of difference potentials is based on finite differences, yet overcomes the method's geometrical limitations using the theory of Calderon's projections [38,37]. The method can also handle variable coefficients, nonstandard boundary conditions, and inhomogeneous media in a straightforward manner. The method supports the use of compact finite difference schemes [9,41,8,40,20], which are beneficial because they allow high-order accuracy without requiring any artificial boundary conditions. In the formulation presented here, we use a compact fourth order scheme for the Helmholtz equation [40].

The fundamental idea of the method is to reduce a differential equation over Ω to an operator equation on the boundary $\Gamma = \partial\Omega$. The resulting boundary operator equation is combined with the boundary condition on Γ, which yields a boundary formulation equivalent to the original BVP on Ω. The boundary operator equation is stated in terms of Calderon's projections and referred to as the Boundary Equation with Projection (BEP). The BEP relates the Dirichlet and Neumann boundary data of the solution and is convenient to combine with the boundary condition that is also formulated in terms of the Dirichlet and/or Neumann boundary data. The BEP is discretized by introducing a finite basis expansion for the Dirichlet and Neumann data and enforcing the equation on a discrete boundary γ that straddles the continuous boundary Γ. The Calderon's projections in the continuous BEP are replaced with difference projections, their discrete analog. A difference projection is computed by solving the auxiliary problem (AP), a Helmholtz boundary value problem on an auxiliary domain Ω_0 that contains Ω, see Fig. 3. The auxiliary domain Ω_0 should not be confused with the intermediate domain Ω_{int} from the regularization algorithm of Section 2. A difference projection is computed for each basis function, so the auxiliary problem must be solved repeatedly. Solution of the discretized BEP yields the unknown boundary data; for example, if the Dirichlet data is specified by the boundary condition, then solution of the BEP yields the Neumann data. Once both types of boundary data are known, the solution is computed throughout Ω in the form of a difference potential.

The current section is not meant to be a comprehensive account of the method of difference potentials [38]. Instead, it is meant to summarize the computational algorithm with special attention paid to the modifications that are required to handle domains with reentrant corners. Other than the modification to the equation-based extension of Section 3.6, the difference potentials formulation presented here does not differ from previously published accounts of the method in any substantial way. For more information on the method of difference potentials, we refer the reader to [31], which may be

considered an introduction. The additional works [32,11,10,33] address transmission/scattering problems, singularities due to discontinuous boundary data, nonstandard boundary conditions, and multiple scattering, respectively.

We apply the method of difference potentials to the Helmholtz boundary value problem

$$\Delta u + k^2 u = f \quad \text{on } \Omega, \tag{58a}$$

$$u\big|_{\Gamma_1} = \varphi_1, \quad u\big|_{\Gamma_2} = \varphi_2, \quad u\big|_{\Gamma_3} = \varphi_3, \tag{58b}$$

where the domain Ω and boundary $\Gamma = \Gamma_1 \cup \Gamma_2 \cup \Gamma_3$ are as defined in Section 1.1. As before, the wavenumber k is assumed constant. While we are reusing the symbols u, f, φ_1, φ_2, and φ_3, it must be understood that BVP (58) is distinct from the BVP (1). In particular, the solution to BVP (1) may well be singular, but we require that (58) have a sufficiently regular solution. This is to say, first the regularization algorithm of Section 2 should be applied to the original problem (1), and then the method of difference potentials can be applied to the regularized problem (57). Rather than use the cumbersome notation of the regularized problem (57), we have returned to the simpler notation (58). The rest of this section addresses the components of the algorithm in the following order: the fourth order compact scheme (Section 3.1), the auxiliary problem (Section 3.2), the discretization grids (Section 3.3), difference potentials and the BEP (Section 3.4), the basis expansion (Section 3.5), and finally the equation-based extension (Section 3.6).

3.1. The compact finite difference scheme

At its core, the method of difference potentials relies on finite difference schemes to approximate the PDE. We employ a fourth order compact equation-based scheme for the Helmholtz equation in Cartesian coordinates:

$$\begin{aligned}
&\frac{u_{i+1,j} - 2u_{i,j} + u_{i-1,j}}{h^2} + \frac{u_{i,j+1} - 2u_{i,j} + u_{i,j-1}}{h^2} + k^2 u_{i,j} \\
&+ \frac{1}{6h^2}\Big[(u_{i+1,j+1} - 2u_{i+1,j} + u_{i+1,j-1}) - 2(u_{i,j+1} - 2u_{i,j} + u_{i,j-1}) \\
&+ (u_{i-1,j+1} - 2u_{i-1,j} + u_{i-1,j-1})\Big] \\
&+ \frac{k^2}{12}\Big[(u_{i+1,j} - 2u_{i,j} + u_{i-1,j}) + (u_{i,j+1} - 2u_{i,j} + u_{i,j-1})\Big] \\
&= \frac{1}{12}(f_{i+1,j} - 2f_{i,j} + f_{i-1,j}) + \frac{1}{12}(f_{i,j+1} - 2f_{i,j} + f_{i,j-1}) + f_{i,j}.
\end{aligned} \tag{59}$$

The scheme is analyzed in [40,20] and has been applied successfully within the framework of difference potentials in [31]. The scheme is referred to as compact because it uses a small 3×3 stencil for the discrete solution $u_{i,j} := u(x_i, y_j)$. That is, to apply the scheme at the node (i, j), only the values of the solution at the nodes $\mathbb{N}_{i,j} = \{(i + \Delta i, j + \Delta j) : \Delta i, \Delta j = -1, 0, 1\}$ are needed. The five node stencil $\mathbb{K}_m = \{(i \pm 1, j), (i, j), (i, j \pm 1)\}$ is applied to the discrete right-hand side $f_{i,j} := f(x_i, y_j)$. High-order accuracy is possible on the compact 3×3 stencil because the Helmholtz equation itself is used to eliminate the leading terms of the truncation error.

3.2. Auxiliary problem

The discretized BEP is generated through repeated solves of the auxiliary problem (AP), an inhomogeneous Helmholtz BVP formulated on Ω_0. The auxiliary domain Ω_0 contains Ω and should be taken in a shape that will facilitate a simple and efficient numerical solution of the AP. We take Ω_0 to be a square of a side length s centered at the origin, though a disc would also be a reasonable choice. Given a right-hand side g defined on Ω_0, the auxiliary problem is to solve the Helmholtz equation

$$\Delta u + k^2 u = g \qquad \text{on } \Omega_0$$

with appropriate boundary conditions. The boundary conditions can be anything, so long as the resulting boundary value problem is well-posed and has a unique solution for any g. We consider homogeneous Dirichlet boundary conditions on all sides of the auxiliary domain: $u|_{\partial\Omega_0} = 0$. The homogeneous Dirichlet boundary conditions are simple to implement and will allow for an efficient numerical solution using separation of variables and FFT. However, if $-k^2$ coincides with an eigenvalue of the Laplacian Δ on Ω_0 with the same homogeneous boundary conditions, then there is a resonance and the solution to the AP will not be unique. The resonance can be avoided by choosing the side length s of the auxiliary domain such that $k^2 \neq \left(\frac{a\pi}{s}\right)^2 + \left(\frac{b\pi}{s}\right)^2$ for any $a, b = 1, 3, 5, \ldots$. Alternatively, in [10,33], the AP is formulated with Sommerfeld-type boundary conditions on the left and right edges of Ω_0 and homogeneous Dirichlet boundary conditions on the upper and lower edges. The Sommerfeld-type BCs make the spectrum of the Laplacian complex so that the purely real number $-k^2$ will never coincide with a Laplacian eigenvalue. However, there are drawbacks associated with the Sommerfeld-type BCs, which require more effort to accurately discretize and prevent us from solving the discrete problem using FFT in the x-direction.

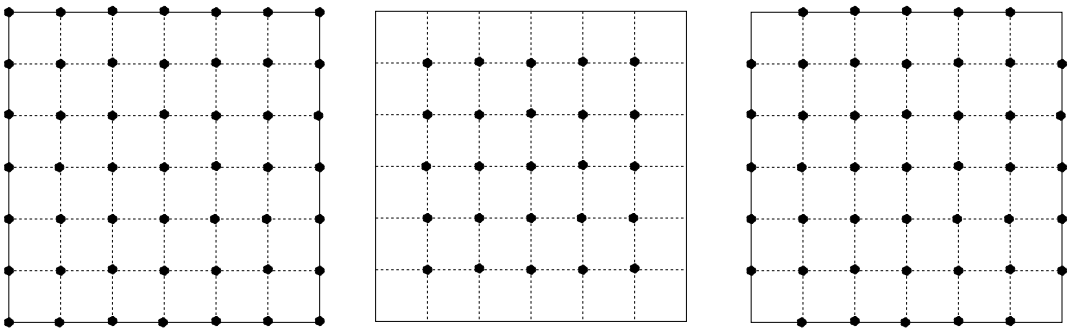

(a) $\mathbb{N}_0$ (b) $\mathbb{M}_0$ (c) $\mathbb{K}_0$

Fig. 4. Discretization grids for the compact scheme.

We define several discretization grids on Ω_0 so that we can formally apply the finite difference scheme (59) to solving the AP. Let $\mathbb{N}_0 = \{(i, j) : i, j = 0, \dots, N\}$ and consider the subsets $\mathbb{M}_0$ and $\mathbb{K}_0$ depicted in Fig. 4. In general the horizontal and vertical spacing of the grid is allowed to differ, but for convenience we take the same step size $h = s/N$ in both directions, so that the coordinates corresponding to the node (i, j) of $\mathbb{N}_0$ are $x_i = -s/2 + ih$ and $y_j = -s/2 + jh$. Enforcing the finite difference approximation (59) of $\Delta u + k^2 u = f$ at the interior nodes $\mathbb{M}_0$ yields a linear system, which we represent symbolically as

$$\boldsymbol{L}^{(h)}\mathfrak{u} = \boldsymbol{B}^{(h)}\mathfrak{f}. \tag{60}$$

Here $\mathfrak{u} = (u_m)_{m\in\mathbb{N}_0}$ is the discrete solution over the grid $\mathbb{N}_0$ and $\mathfrak{f} = (f_m)_{m\in\mathbb{K}_0}$ is the discrete right-hand side. Clearly, there are more unknowns than equations, so the system (60) requires an additional constraint, which comes from the discrete boundary conditions

$$u_{i,0} = u_{i,N} = u_{j,0} = u_{j,N} = 0, \qquad i, j = 0, \dots, N. \tag{61}$$

Then, for a given function $\mathfrak{g}$ on $\mathbb{M}_0$, the discrete auxiliary problem is to solve the system

$$\boldsymbol{L}^{(h)}\mathfrak{u} = \mathfrak{g} \tag{62}$$

subject to the boundary conditions (61). Since the boundary conditions are homogeneous and Dirichlet, the discrete AP (62) can be solved efficiently with FFT. The discrete AP will be solved repeatedly throughout the algorithm, so it is convenient to introduce notation for the solution operator. Let $\boldsymbol{G}^{(h)}$ be the Green's function for the discrete AP, so that $\boldsymbol{G}^{(h)}\mathfrak{g}$ denotes the solution $\mathfrak{u}$ to the linear system $\boldsymbol{L}^{(h)}\mathfrak{u} = \mathfrak{g}$ for the given function $\mathfrak{g}$.

3.3. Grid sets

The method of difference potentials works by enforcing the BEP at the boundary, yet in general the boundary Γ does not conform to the grid. Therefore we will instead enforce the BEP at a discrete boundary γ that straddles the continuous boundary Γ. Towards this end, we partition $\mathbb{M}_0$ into the set of nodes $\mathbb{M}^+ = \mathbb{M}_0 \cap \Omega$ that lie inside the domain, and the set $\mathbb{M}^- = \mathbb{M}_0 \cap \Omega$ which lie outside. The discrete boundary γ is defined by applying the 3×3 stencil $\mathbb{N}_m$ at each node m of $\mathbb{M}^+$ and $\mathbb{M}^-$, and then taking the intersection:

$$\mathbb{N}^+ = \bigcup_{m\in\mathbb{M}^+} \mathbb{N}_m, \qquad \mathbb{N}^- = \bigcup_{m\in\mathbb{M}^-} \mathbb{N}_m, \qquad \gamma = \mathbb{N}^+ \cap \mathbb{N}^-.$$

The interior, exterior, and boundary grid sets are shown schematically in Fig. 5. Additionally, let us define yet another grid set, this time in terms of the five node stencil $\mathbb{K}_m$ on the right-hand side:

$$\mathbb{K}^+ = \bigcup_{m\in\mathbb{M}^+} \mathbb{K}_m.$$

Computing $\boldsymbol{B}^{(h)}\mathfrak{f}$ at a given interior node $m \in \mathbb{M}^+$ makes use of the values of $\mathfrak{f}$ at the adjacent nodes $\mathbb{K}_m$, so naturally $\mathfrak{f}$ must be defined on a larger grid $\mathbb{K}^+$ that contains the interior nodes $\mathbb{M}^+$ as well as a fringe of nodes slightly outside the domain.

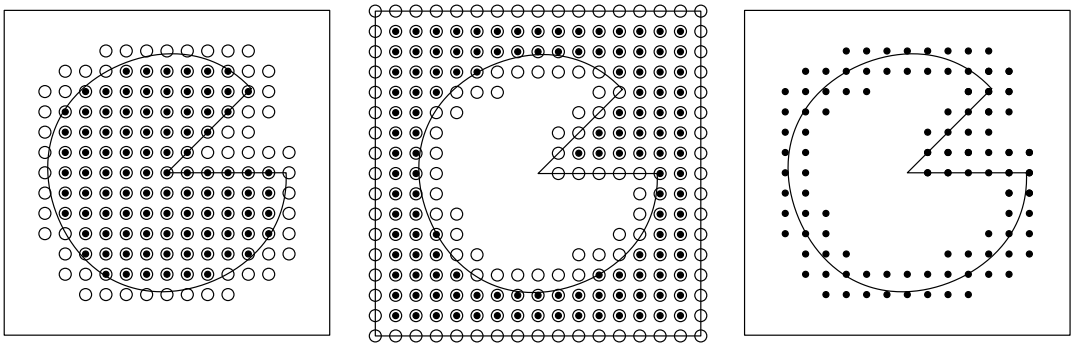

(a) • – $\mathbb{M}^+$, ◯ – $\mathbb{N}^+$. (b) • – $\mathbb{M}^-$, ◯ – $\mathbb{N}^-$. (c) • – γ.

Fig. 5. The interior, exterior, and boundary grid sets for the wedge angle $\alpha = \pi/4$.

3.4. Difference potentials

At last, we are ready to define the term difference potential. Again, we refer the reader to [31] for in-depth coverage of difference potentials and projections, especially for the continuous case. Let ξ_γ be a given function on the grid γ. Let w be a function on $\mathbb{N}_0$ such that its trace $\boldsymbol{Tr}^{(h)} w$ on the discrete boundary coincides with ξ_γ,

$$\boldsymbol{Tr}^{(h)} w = \xi_\gamma .$$

Then the difference potential with density ξ_γ is a function on $\mathbb{N}^+$ defined by

$$\boldsymbol{P}_{\mathbb{N}^+}\xi_\gamma = w - \boldsymbol{G}^{(h)}\left(\boldsymbol{L}^{(h)} w\big|_{\mathbb{M}^+}\right),$$

where $\boldsymbol{L}^{(h)}$ is the fourth order approximation of the Helmholtz operator, see (60), and $\boldsymbol{G}^{(h)}$ is the solution operator to the discrete AP (62). The notation $\boldsymbol{L}^{(h)} w\big|_{\mathbb{M}^+}$ means that the operator $\boldsymbol{L}^{(h)}$ should be applied to w, and then the result should be set to 0 at nodes not in $\mathbb{M}^+$. Next, we introduce the notation $\boldsymbol{P}_\gamma$ for the difference boundary projection, obtained by restricting the difference potential to the discrete boundary:

$$\boldsymbol{P}_\gamma \xi_\gamma = \boldsymbol{Tr}^{(h)} \boldsymbol{P}_{\mathbb{N}^+}\xi_\gamma . \tag{63}$$

Then discrete boundary equation with projection (BEP) is stated in terms of the projection (63),

$$\boldsymbol{P}_\gamma \xi_\gamma + \boldsymbol{Tr}^{(h)} \boldsymbol{G}^{(h)} \boldsymbol{B}^{(h)} \mathfrak{f} = \xi_\gamma , \tag{64}$$

where $\mathfrak{f}$ is an extension of the right-hand side f of the Helmholtz equation (58a) to the larger grid $\mathbb{K}^+ \supset \mathbb{M}^+$. The fundamental property of the discrete BEP is that ξ_γ satisfies (64) if and only if there exists a grid function $\mathfrak{u}$ with $\boldsymbol{Tr}^{(h)}\mathfrak{u} = \xi_\gamma$ that satisfies $\boldsymbol{L}^{(h)}\mathfrak{u} = \boldsymbol{B}^{(h)}\mathfrak{f}$ on $\mathbb{M}^+$. Finally, the solution $\mathfrak{u}$ is obtained through use of the formula

$$\mathfrak{u} = \boldsymbol{P}_{\mathbb{N}^+}\xi_\gamma + \boldsymbol{G}^{(h)} \boldsymbol{B}^{(h)} \mathfrak{f}. \tag{65}$$

Thus, the BEP reduces the problem $\boldsymbol{L}^{(h)}\mathfrak{u} = \boldsymbol{B}^{(h)}\mathfrak{f}$ over the set of interior nodes $\mathbb{M}^+$ to a problem at the discrete boundary γ.

There are many functions ξ_γ that satisfy the discrete BEP (64), just as there are many functions $\mathfrak{u}$ that satisfy the discretization $\boldsymbol{L}^{(h)}\mathfrak{u} = \boldsymbol{B}^{(h)}\mathfrak{f}$ of the PDE on the interior nodes $\mathbb{M}^+$. To make the BEP uniquely solvable, we must involve the boundary conditions on $\Gamma = \partial\Omega$, yet the BEP is enforced at the fringe of nodes γ rather than on the continuous boundary Γ. We bridge the gap by expanding the boundary data relative to a finite set of basis functions, and then applying the equation-based extension. Consider the vector-valued function $\boldsymbol{\xi}_\Gamma = (\xi_0, \xi_1)|_\Gamma$ that represents the trace of the solution u to the Helmholtz equation (58a) and its outwards normal derivative $\frac{\partial u}{\partial n}$ on the boundary. Given the density $\boldsymbol{\xi}_\Gamma$ of the solution u, the equation-based extension defines an approximation $\boldsymbol{Ex}\boldsymbol{\xi}_\Gamma$ of u at the discrete boundary γ. It is the extension $\boldsymbol{Ex}\boldsymbol{\xi}_\Gamma$ that takes the place of ξ_γ in the BEP.

3.5. Expansion of boundary data

Initially, the density $\boldsymbol{\xi}_\Gamma$ corresponding to the solution is not entirely known. For the Dirichlet boundary conditions (58b) considered here, the Dirichlet data ξ_0 is known, while the Neumann data ξ_1 is unknown. To include the unknown Neumann data in the BEP, we expand the vector function $\boldsymbol{\xi}_\Gamma$ with respect to a Chebyshev basis on each of the boundary segments $\Gamma_1, \Gamma_2, \Gamma_3$. The Chebyshev polynomials are defined on $[-1, 1]$, so we introduce the linear functions g_j, $j = 1, 2, 3$ that map $[-1, 1]$ onto the segment Γ_j. The radii Γ_1 and Γ_2 are parameterized by the polar radius r, so g_1 and g_2 should return values

of r. Likewise, the outer boundary Γ_3 is parameterized by θ, so g_3 should return values of θ. In either case, the parameter (r or θ) can take on any value in a certain interval $[b_0, B_0]$ ($[0, R]$ or $[\alpha, 2\pi]$ respectively). If we take g_j to be a bijection from $[-1, 1]$ to the interval $[b_0, B_0]$, then the endpoints of the boundary segments will correspond to endpoints of $[-1, 1]$, where the derivatives of the Chebyshev polynomials are large. In previous numerical experiments, we have observed a loss of accuracy when these large derivative values enter into the extension procedure. The solution is to have g_j map $[-1, 1]$ into the slightly larger interval $[b_0 - \varepsilon, B_0 + \varepsilon]$, for a small positive number ε, e.g. $\varepsilon = 10^{-3}$ in our experiments. Then, the functions g_j can be taken in the form $g_j(t) = C_j t + D_j$, $j = 1, 2, 3$ with

$$C_1 = C_2 = \frac{R}{2} + \varepsilon \qquad C_3 = \pi - \frac{\alpha}{2} + \varepsilon$$
$$D_1 = D_2 = \frac{R}{2} \qquad D_3 = \pi + \frac{\alpha}{2}.$$

We also consider the inverse functions g_j^{-1}, given by $g_j^{-1}(a) = (a - D_j)/C_j$.

Next, we define the vector-valued basis functions in terms of the Chebyshev polynomials $\{T_n\}$. For the radii Γ_j, $j = 1, 2$, the basis sets for the Dirichlet data ξ_0 and the Neumann data ξ_1 are

$$\boldsymbol{\psi}_n^{(0,j)}(r,\theta) = \begin{cases} (T_n(g_j^{-1}(r), 0)) & \text{on } \Gamma_j \\ (0,0) & \text{on } \Gamma \setminus \Gamma_j \end{cases},$$
$$\boldsymbol{\psi}_n^{(1,j)}(r,\theta) = \begin{cases} (0, T_n(g_j^{-1}(r))) & \text{on } \Gamma_j \\ (0,0) & \text{on } \Gamma \setminus \Gamma_j \end{cases}, \qquad n = 0, 1, \ldots,$$

respectively. The definition is the same for the outer boundary, except with the Chebyshev functions parameterized by θ rather than r:

$$\boldsymbol{\psi}_n^{(0,3)}(r,\theta) = \begin{cases} (T_n(g_3^{-1}(\theta), 0)) & \text{on } \Gamma_3 \\ (0,0) & \text{on } \Gamma \setminus \Gamma_3 \end{cases},$$
$$\boldsymbol{\psi}_n^{(1,3)}(r,\theta) = \begin{cases} (0, T_n(g_3^{-1}(\theta))) & \text{on } \Gamma_3 \\ (0,0) & \text{on } \Gamma \setminus \Gamma_3 \end{cases}, \qquad n = 0, 1, \ldots.$$

Then we can represent the vector density $\boldsymbol{\xi}_\Gamma$ as

$$\boldsymbol{\xi}_\Gamma = \underbrace{\sum_{j=1}^{3} \sum_{n=0}^{N_j - 1} c_n^{(0,j)} \boldsymbol{\psi}_n^{(0,j)}}_{(\xi_0, 0)} + \underbrace{\sum_{j=1}^{3} \sum_{n=0}^{N_j - 1} c_n^{(1,j)} \boldsymbol{\psi}_n^{(1,j)}}_{(0, \xi_1)}, \tag{66}$$

where N_j denotes the number of basis functions on the segment Γ_j. We are using a finite number of Chebyshev polynomials, so the expansion (66) is only an approximation of the density $\boldsymbol{\xi}_\Gamma$. However, the Chebyshev expansion converges rapidly, so there will be no loss of accuracy when the number of basis functions N_j, $j = 1, 2, 3$ is set appropriately; see Section 4. The coefficients $\{c_n^{(1,j)}\}$ are unknown and are included in the BEP. On the other hand, the Dirichlet data ξ_0 is given by the boundary condition, so the coefficients $\{c_n^{(0,j)}\}$ are considered known quantities.[7] In practice, these coefficients are obtained by performing a Chebyshev fit on each segment of the boundary. The functions g_j map the Chebyshev polynomials to the larger interval $[b_0 - \varepsilon, B_0 + \varepsilon]$, so the functions φ_j, $j = 1, 2, 3$ which supply the boundary data must be smoothly extended to this larger set.

The grid function ξ_γ is defined by the equation-based extension, which has a homogeneous component from the boundary data (ξ_0, ξ_1) and an inhomogeneous component from the source term f. Then, we may write

$$\xi_\gamma = \boldsymbol{Ex}\boldsymbol{\xi}_\Gamma = \boldsymbol{Ex}_H(\xi_0, \xi_1)|_\Gamma + \boldsymbol{Ex}_I f, \tag{67}$$

where $\boldsymbol{Ex}_H$ and $\boldsymbol{Ex}_I$ denote the homogeneous and inhomogeneous components of the extension. Replacing $\boldsymbol{\xi}_\Gamma$ with its expansion (66) and using the linearity of the extension, we see that

$$\xi_\gamma = \sum_{j=1}^{3} \sum_{n=0}^{N_j - 1} c_n^{(0,j)} \boldsymbol{Ex}_H \boldsymbol{\psi}_n^{(0,j)} + \sum_{j=1}^{3} \sum_{n=0}^{N_j - 1} c_n^{(1,j)} \boldsymbol{Ex}_H \boldsymbol{\psi}_n^{(1,j)} + \boldsymbol{Ex}_I f. \tag{68}$$

[7] It is not even truly necessary to expand the known Dirichlet data ξ_0 with respect to the basis, since the extension and difference projections can be computed for ξ_0 itself rather than the individual basis functions. Such an approach will significantly reduce the computational cost, though it does not generalize to more complex boundary conditions and requires that the particular functions φ_1, φ_2, and φ_3 for each problem be differentiated ahead of time, either manually or symbolically.

Then, substitution of (68) into the discrete BEP (64) yields the following linear system:

$$\sum_{j=1}^{3} Q^{(1,j)} \boldsymbol{c}^{(1,j)} = -\sum_{j=1}^{3} Q^{(0,j)} \boldsymbol{c}^{(0,j)} - \boldsymbol{T}\boldsymbol{r}^{(h)} \boldsymbol{G}^{(h)} \boldsymbol{B}^{(h)} \mathfrak{f}, \tag{69}$$

where the vectors of coefficient are defined by

$$\boldsymbol{c}^{(i,j)} = \left[c_0^{(i,j)}, \ldots, c_{N_j-1}^{(i,j)} \right], \quad i = 0, 1, \quad j = 1, 2, 3.$$

Here, $i = 0$ and $i = 1$ correspond to the Dirichlet and Neumann data respectively. The matrices $Q^{(0,j)}$ and $Q^{(1,j)}$ are defined in terms of their columns,

$$Q^{(i,j)} = \left[(\boldsymbol{P}_\gamma - \boldsymbol{I}) \boldsymbol{E}\boldsymbol{x}_H \boldsymbol{\psi}_n^{(i,j)} \right]_{n=0}^{N_j-1}, \quad i = 0, 1, \quad j = 1, 2, 3.$$

In the system (69), the Neumann coefficients $\boldsymbol{c}^{(1,j)}$, $j = 1, 2, 3$ are unknown, while the other terms are known. In particular, the Dirichlet coefficients $\boldsymbol{c}^{(0,j)}$, $j = 1, 2, 3$ have been obtained by performing a Chebyshev fit on each segment. The linear system (69) has one equation per each node of γ and $N_1 + N_2 + N_3$ unknowns. For reasonable choices of the grid dimension and the sizes N_1, N_2, N_3 of the basis sets, we have $|\gamma| > N_1 + N_2 + N_3$, so that system (69) is overdetermined. Thus, we are seeking its weak solution in the sense of least squares. Nevertheless, the weak solution to system (69) will be "almost classical", in that each equation is approximately satisfied, up to the accuracy of the discrete approximation. Solving system (69) gives the coefficients $\boldsymbol{c}^{(1,j)}$, $j = 1, 2, 3$ which approximate the Neumann boundary data of the solution to the boundary value problem. Once this Neumann data is available, the solution is computed in the interior of Ω via formula (65).

3.6. The equation-based extension

The equation-based extension constructs an approximation of the solution u to the Helmholtz equation (58a) on the discrete boundary γ given its vector density $\boldsymbol{\xi}_\Gamma$. Such an extension is necessary to incorporate the boundary conditions into the BEP, which is formulated at the discrete boundary γ. The extension is the area in which the version of the method of difference potentials presented here differs most from the standard formulation for domains without corners.

3.6.1. Smooth boundaries

The extension is built with the help of an alternate coordinate system that specifies the position of the node $m \in \gamma$ relative to the curve Γ. We begin by describing the new coordinate system in the case when Γ is smooth, and then move on to the more difficult case in which there are corners. Let Γ be parameterized by its arc length, $\Gamma = \{\boldsymbol{R}(s) : 0 \le s \le S\}$, where $\boldsymbol{R}(s)$ is the radius vector. Then the coordinates of the node $m \in \gamma$ are obtained by finding the point E_m on Γ that minimizes the distance $\|E_m - m\|_2$. The point E_m is unique when Γ has sufficiently low curvature, and can be identified by "dropping a normal" from m to the boundary. Let n denote the signed length of the normal, with n positive when the normal points outward with respect to Ω, and negative when the normal points inward. Additionally, let s be the value of the arc length parameter such that $E_m = \boldsymbol{R}(s)$. Then the ordered pair (n, s) are the coordinates associated with Γ for the node m. In practice, a root-finding algorithm like Newton's method is used to calculate the coordinates (n, s).

Near Γ, we define a new function $v(n, s)$ in the form of a Taylor polynomial,

$$v(n, s) = v(0, s) + \sum_{l=1}^{L} \frac{1}{l!} \frac{\partial^l v(0, s)}{\partial n^l} n^l, \tag{70}$$

where $v(0, s)$ and each of the normal derivatives $\frac{\partial^l v(0,s)}{\partial n^l}$ are calculated from the boundary data $\boldsymbol{\xi}_\Gamma$. Suppose the node $m \in \gamma$ has coordinates (n, s). Then, the value of the equation-based extension at m is given by $v(n, s)$. The extension is referred to as "equation-based" because the formulas for the higher derivatives $\frac{\partial^l v(0,s)}{\partial n^l}$, $l = 2, 3, \ldots, L$ are obtained by assuming that v satisfies the Helmholtz equation (58a). In [31], it was found that taking $L = p$ is sufficient when the method has the overall order of accuracy p.[8] Thus, we take $L = 4$ in our implementation of the algorithm and present the formulas for the partial derivatives of v up to $\frac{\partial^4 v(0,s)}{\partial n^4}$.

The first two terms in the Taylor polynomial (70) are obtained directly from the density $\boldsymbol{\xi}_\Gamma = (\xi_0, \xi_1)|_\Gamma$,

$$v(0, s) = \xi_0(s), \qquad \frac{\partial v(0, s)}{\partial n} = \xi_1(s).$$

[8] This finding is experimental. In [36], a more strenuous requirement was proven rigorously: $L = p + 2$, where 2 represents the order of the differential equation.

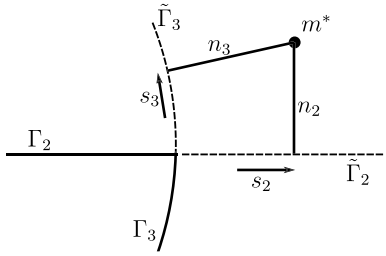

Fig. 6. Extension to a node near the corner formed by Γ_2 and Γ_3.

The formulas for the higher order derivatives are obtained by rewriting the Helmholtz equation (58a) in terms of the coordinates (n, s), with the help of Lamé coefficients. This analysis has already been carried out in [33], so we shall state the results without repeating the derivation. First, we introduce a unit tangent $\boldsymbol{\tau} = \boldsymbol{\tau}(s)$ and a unit normal $\boldsymbol{\nu} = \boldsymbol{\nu}(s)$ of the boundary Γ. We assume the arc length parameterization $\boldsymbol{R}(s)$ is counterclockwise, so that the unit normal $\boldsymbol{\nu}$ always points outwards. Then, the signed curvature is

$$\zeta(s) = \begin{cases} \left|\dfrac{d\boldsymbol{\tau}}{ds}\right|, & \text{if } \dfrac{d\boldsymbol{\tau}}{ds} \cdot \boldsymbol{\nu} > 0, \\ -\left|\dfrac{d\boldsymbol{\tau}}{ds}\right|, & \text{if } \dfrac{d\boldsymbol{\tau}}{ds} \cdot \boldsymbol{\nu} < 0. \end{cases}$$

The second and third derivatives in the Taylor polynomial are given by

$$\frac{\partial^2 v(0,s)}{\partial n^2} = f(0,s) - k^2 \xi_0(s) + \zeta(s)\xi_1(s) - \frac{\partial^2 \xi_0(s)}{\partial s^2},$$
$$\frac{\partial^3 v(0,s)}{\partial n^3} = \frac{\partial f(0,s)}{\partial n} + \left(\zeta^2 - k^2\right)\xi_1(s) + \zeta \frac{\partial^2 v(0,s)}{\partial n^2} - \zeta' \frac{\partial \xi_0(s)}{\partial s} - 2\zeta \frac{\partial^2 \xi_0(s)}{\partial s^2} - \frac{\partial^2 \xi_1(s)}{\partial s^2}.$$

The paper [33] allowed the wavenumber k to vary in space, so the expressions for the derivatives included contributions from the partial derivatives of $k(n, s)$. We have dropped these terms, since we assume a constant wavenumber. The fourth derivative is

$$\frac{\partial^4 v(0,s)}{\partial n^4} = \frac{\partial^2 f(0,s)}{\partial n^2} + 2\zeta^3 \xi_1(s) + \left(2\zeta^2 - k^2\right)\frac{\partial^2 v(0,s)}{\partial n^2} + \zeta \frac{\partial^3 v(0,s)}{\partial n^3}$$
$$- 6\zeta\zeta' \frac{\partial \xi_0(s)}{\partial s} - 6\zeta^2 \frac{\partial^2 \xi_0(s)}{\partial s^2} - 2\zeta' \frac{\partial \xi_1(s)}{\partial s} - 4\zeta \frac{\partial^2 \xi_1(s)}{\partial s^2} - \frac{\partial^4 v(0,s)}{\partial n^2 \partial s^2},$$

where, for the final term, we have

$$\frac{\partial^4 v(0,s)}{\partial n^2 \partial s^2} = \frac{\partial^2 f(0,s)}{\partial s^2} + \zeta'' \xi_1(s) - k^2 \frac{\partial^2 \xi_0(s)}{\partial s^2} - \frac{\partial^4 \xi_0(s)}{\partial s^4} + 2\zeta' \frac{\partial \xi_1(s)}{\partial s} + \zeta \frac{\partial^2 \xi_1(s)}{\partial s^2}.$$

Thus, all terms of the Taylor series (70) can be computed from $\boldsymbol{\xi}_\Gamma = (\xi_0, \xi_1)|_\Gamma$, the right-hand side f, and their partial derivatives. For the homogeneous component $\boldsymbol{E}\boldsymbol{x}_H$ of the extension, introduced in (67), the formulas for $\frac{\partial^l v(0,s)}{\partial n^l}$ should be evaluated with $f \equiv 0$ so that only the terms involving ξ_0 and ξ_1 make a contribution. Similarly, for the inhomogeneous $\boldsymbol{E}\boldsymbol{x}_I$, the partials of v should be computed with $\xi_0, \xi_1 \equiv 0$, leaving only the contributions from f.

3.6.2. Boundaries with corners

The coordinates (n, s) are defined unambiguously for each node of γ when the continuous boundary is smooth and has sufficiently low curvature. But the situation is less clear when the boundary has corners. Consider the node denoted by m^* in Fig. 6. We can still identify the point E_{m^*} on Γ that is closest to m^*, but the vector from E_{m^*} to m^* will not be normal to the boundary, meaning that formula (70) cannot be used directly. An additional question arises when we recognize that there are independent systems of basis functions on each of the two segments that meet to form the corner. Consider Fig. 6: if we use the boundary data on Γ_2 when extending to m^*, then the corresponding equation in system (69) will be in terms of the coefficients $\boldsymbol{c}^{(2)}$. On the other hand, if we use the boundary data on Γ_3, then this equation will be in terms of $\boldsymbol{c}^{(3)}$. We expect this choice to matter, since always choosing to use the coefficients $\boldsymbol{c}^{(3)}$, for example, would cause there to be no constraints on $\boldsymbol{c}^{(2)}$ near the corner, thus decreasing the accuracy with which system (69) can reconstruct the unknown Neumann data.

There are likely multiple ways to resolve these issues and define the extension for nodes near the interfaces of two segments. The method we present has been found to work in practice. As illustrated in Fig. 6, the shortest vector between a given node of γ and the boundary may fail to be normal to the boundary. We address this problem by creating smooth

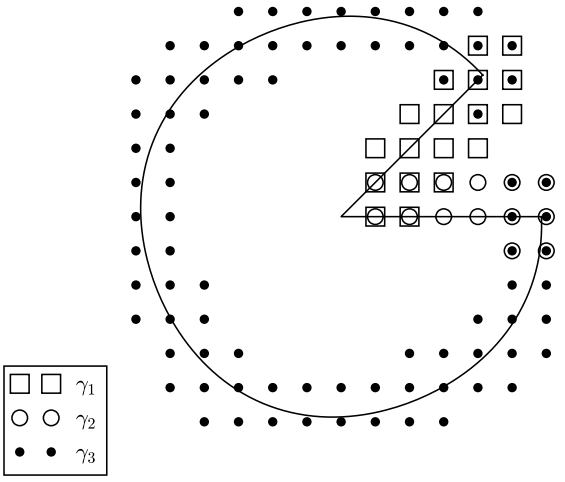

Fig. 7. γ_1, γ_2, and γ_3 for $\alpha = \pi/4$ on a 16×16 grid.

extensions $\tilde{\Gamma}_1, \tilde{\Gamma}_2, \tilde{\Gamma}_3$ of each segment of the boundary. If Γ_j, $j = 1, 2, 3$ is the curve $\{\boldsymbol{R}_j(s) : 0 \le s \le S_j\}$, then its extension is

$$\tilde{\Gamma}_j = \{\tilde{\boldsymbol{R}}_j(s) : -\rho_j \le s \le S_j + \rho_j\}$$

for some $\rho_j > 0$, with $\tilde{\boldsymbol{R}}_j$ an extension of $\boldsymbol{R}_j$. Then, the coordinates (n_j, s_j) associated with the curve $\tilde{\Gamma}_j$ can be defined even for nodes like m^* of Fig. 6, provided that ρ_j is large enough. The coordinates are given the subscript $j \in \{1, 2, 3\}$ to emphasize that nodes near the interface of two segments will be associated with two different segments and thus have two sets of coordinates. More precisely, we define the set of nodes associated with the segment Γ_j as

$$\gamma_j = \left\{ m \in \gamma \ : \ \operatorname{dist}(m, \Gamma_j) \le \frac{h}{\sqrt{2}} \right\},$$

where $\operatorname{dist}(m, \Gamma_j) = \inf_{(x,y)\in\Gamma_j} \|m - (x, y)\|_2$. We have chosen the constant $\frac{h}{\sqrt{2}}$ because it is the distance between the central node and the corner nodes in the 3×3 stencil $\mathbb{N}_m$. The sets γ_1, γ_2, and γ_3 are shown in Fig. 7 for a coarse grid.

Previously, we said that there are two choices for building the extension to m^* in Fig. 6, since we can either use the boundary data on Γ_2, or instead use the data on Γ_3. In ambiguous situations like this, our method works by computing both extensions and averaging them. To make this idea formal, we begin by introducing the "segment-specific" extension operator $\boldsymbol{Ex}^j$ for each $j = 1, 2, 3$. Given a density $\boldsymbol{\xi}_{\tilde{\Gamma}_j}$ defined on the extended segment $\tilde{\Gamma}_j$, the operator $\boldsymbol{Ex}^j$ defines a new function on γ_j via the Taylor formula (70) using the coordinates (n_j, s_j) associated with $\tilde{\Gamma}_j$. The terms of the Taylor polynomial (70) should be computed by evaluating the extended density $\boldsymbol{\xi}_{\tilde{\Gamma}_j}$ and its derivatives at the point $(0, s_j)$ on $\tilde{\Gamma}_j$. The extended density $\boldsymbol{\xi}_{\tilde{\Gamma}_j}$ is obtained from $\boldsymbol{\xi}_\Gamma$ using a Taylor approximation. The segment Γ_j is given by $\boldsymbol{R}_j(s_j)$ for $0 \le s_j \le S_j$, so it is natural to parameterize the density in a similar way:

$$\boldsymbol{\xi}_{\tilde{\Gamma}_j} = (\xi_0(s_j), \xi_1(s_j))\Big|_{-\rho_j \le s_j \le S_j + \rho_j}.$$

When $s_j > S_j$, we shall build the Taylor approximation for $\xi_0(s_j), \xi_1(s_j)$ at $s_j^0 := S_j$, the closest point on the original curve Γ_j. In the other case when $s_j < 0$, we build the approximation at $s_j^0 = 0$. Then, the approximation is

$$\xi_0(s_j) = \xi_0(s_j^0) + \sum_{l=1}^{L} \frac{1}{l!} \xi_0^{(l)}(s_j^0)(s_j - s_j^0)^l, \tag{71a}$$

$$\xi_1(s_j) = \xi_1(s_j^0) + \sum_{l=1}^{L} \frac{1}{l!} \xi_1^{(l)}(s_j^0)(s_j - s_j^0)^l, \tag{71b}$$

where the superscript in $\xi_0^{(l)}$, $\xi_1^{(l)}$ denotes the l-th derivative with respect to arc length. The number of derivatives in the extension (71) of the density should be greater than or equal to the number of derivatives in the main extension formula (70) to maintain the overall order of accuracy. We are including up to the L-th derivative in both formulas. Approximations for the derivatives of ξ_0 and ξ_1 with respect to the arc length s_j may be obtained by differentiating the Taylor polynomials (71).

The "global" extension operator $\boldsymbol{Ex}$ is defined in terms of the segment-specific extension operators $\boldsymbol{Ex}^j$, $j = 1, 2, 3$. For nodes that are only associated with a single boundary segment, the global extension and segment-specific extension coincide, while for nodes near the corners, the global extension is the average of two segment-specific extensions. Formally, for each node $m \in \gamma$ we have

$$(\boldsymbol{Ex}\boldsymbol{\xi}_\Gamma)_m = \begin{cases} (\boldsymbol{Ex}^j \boldsymbol{\xi}_{\Gamma_j})_m, & \text{if } m \in \gamma_j \text{ and } m \notin \gamma_i \text{ for any } i \neq j, \\ \frac{1}{2}\left[(\boldsymbol{Ex}^i \boldsymbol{\xi}_{\tilde{\Gamma}_i})_m + (\boldsymbol{Ex}^j \boldsymbol{\xi}_{\tilde{\Gamma}_j})_m\right], & \text{if } m \in \gamma_i \cap \gamma_j,\ i \neq j. \end{cases} \tag{72}$$

In the first case, we write the density as $\boldsymbol{\xi}_{\Gamma_j}$ rather than $\boldsymbol{\xi}_{\tilde{\Gamma}_j}$ to emphasize that there is no need to define the density on an extended segment, since the node m is not near a corner. Near the beginning of this section, we wrote in the context of Fig. 6 that always favoring one segment-specific extension $\boldsymbol{Ex}^i$ over another $\boldsymbol{Ex}^j$ would result in a dearth of constraints on the coefficients $\boldsymbol{c}^{(j)}$ in system (69). By defining the global extension as the average of the two segment-specific extensions $\boldsymbol{Ex}^i$ and $\boldsymbol{Ex}^j$ near the corner, we ensure that an appropriate number of constraints is placed on each of $\boldsymbol{c}^{(i)}$ and $\boldsymbol{c}^{(j)}$. This approach has proven a reasonable solution as it has delivered the expected results in our numerical experiments, see Section 4. The relationship (72) between the global and segment-specific extension operators applies to the homogeneous and inhomogeneous extension operators $\boldsymbol{Ex}_H$ and $\boldsymbol{Ex}_I$ as well. The analog of (72) for the homogeneous and inhomogeneous extensions is obtained by replacing all instances of $\boldsymbol{Ex}$ with $\boldsymbol{Ex}_H$ or $\boldsymbol{Ex}_I$, respectively.

In addition to extending the density $\boldsymbol{\xi}_\Gamma$ to the discrete boundary, we also need to extend the function $\mathfrak{f}$ to the larger grid the larger grid $\mathbb{K}^+ \supset \mathbb{M}^+$ to compute the term $\boldsymbol{Tr}^{(h)}\boldsymbol{G}^{(h)}\boldsymbol{B}^{(h)}\mathfrak{f}$ in system (69). At the interior nodes $\mathbb{M}^+$, we obtain $\mathfrak{f}$ simply by evaluating the source term f of the Helmholtz equation (58a) on the grid: $\mathfrak{f}_{i,j} = f(x_i, y_j)$. For the nodes $\mathbb{K}^+ \setminus \mathbb{M}^+$ which lay slightly outside Ω, $\mathfrak{f}$ is obtained via a smooth extension of f. Such an extension can be calculated, for example, by using the gradient and Hessian of f to construct a Taylor series approximation. While we use a five term Taylor polynomial for the equation-based extension (70), two fewer terms are sufficient for extending f, since it is the right-hand side of a second order differential equation. For the node $(x_i, y_j) \in \mathbb{K}^+ \setminus \mathbb{M}^+$, consider the point $(\tilde{x}, \tilde{y})$ on Γ that minimizes the distance $\delta = \|(x_i, y_j) - (\tilde{x}, \tilde{y})\|_2$, and define the unit vector

$$\boldsymbol{v} = \frac{1}{\delta}\left[(x_i, y_j) - (\tilde{x}, \tilde{y})\right].$$

Then, we can define $\mathfrak{f}_{i,j}$ by means of the Taylor formula

$$\mathfrak{f}_{i,j} = f(\tilde{x}, \tilde{y}) + \delta\, \boldsymbol{v} \cdot \nabla f(\tilde{x}, \tilde{y}) + \frac{\delta^2}{2}\, \boldsymbol{v} \cdot D^2 f(\tilde{x}, \tilde{y}) \cdot \boldsymbol{v}^\intercal,$$

where $D^2 f$ is the Hessian of f.

4. Numerical results

In this section, we present the convergence results for the algorithm for various choices of the boundary data and outer boundary. For all of our experiments, we take the length R of the radial segments Γ_1 and Γ_2 to be 2.3. We consider two choices for the wedge angle, $\alpha = \pi/6$ and $\alpha = \pi/2$. The outer boundary is specified by the function $r_3(\theta)$, $\alpha \le \theta \le 2\pi$, so we introduce Boundaries A, B, C, and D by defining the corresponding functions $r_3 = r_3(\theta)$ [cf. formula (49)]:

$$\begin{aligned}
&\text{A:} \quad r_3(\theta) = R - \beta \sin(\nu(\theta - \alpha)), \quad \beta = 0.5, \\
&\text{B:} \quad r_3(\theta) = R + \frac{\beta}{\kappa}(\theta - \alpha)(\theta - \pi)(\theta - 2\pi), \quad \kappa = \frac{(91\sqrt{91} - 136)\pi^3}{2916}, \quad \beta = 0.075, \\
&\text{C:} \quad r_3(\theta) = R + \beta \sin(\nu(\theta - \alpha)), \quad \beta = 0.15, \\
&\text{D:} \quad r_3(\theta) = R + \beta \sin(7\nu(\theta - \alpha)), \quad \beta = 0.025.
\end{aligned}$$

The parameter $\beta = \max_{\alpha \le \theta \le 2\pi} |r_3(\theta) - R|$ given by formula (50) quantifies the magnitude of deviation of the true boundary Γ_3 for the arc $r = R$. Thus we see that Boundary A ($\beta = 0.5$) has the largest deviation, while Boundary D ($\beta = 0.025$) has the smallest.[9] The extension procedure requires the creation of extensions $\tilde{\Gamma}_1$, $\tilde{\Gamma}_2$, $\tilde{\Gamma}_3$ of the boundary segments. The segments Γ_1 and Γ_2 are line segments, so it is natural to take the corresponding extended segments to be line segments as well. The extended outer boundary $\tilde{\Gamma}_3$ is defined by the same function $r_3 = r_3(\theta)$ that describes Γ_3, except we allow θ to take on values slightly outside the interval $[\alpha, 2\pi]$. For the intermediate domain that features in the regularization algorithm, see Fig. 2, we take $R_0 = 0.1$ for the inner radius and $R_{\text{arc}} = R + \beta$ for the outer radius. We set $s = 2\pi$ for the side length of the square auxiliary domain Ω_0, shown in Fig. 3.

[9] For small values of β, the boundary Γ_3 can be considered a perturbation of the arc $r = R$. In that regard we note that the idea of considering the general boundary as a perturbation of a regular shape has proven useful for computing the Dirichlet-to-Neumann maps and constructing the artificial boundary conditions for the numerical simulation of the scattering of waves, see, e.g., [34,35,13,7].

Table 1
Convergence results and the sizes of the basis sets for boundary value problem (73) with $k = 6.75$ and $\alpha = \pi/6$.

Grid	Convergence rate			Basis dimensions	
	Boundary A $\varphi_2(r) = J_{\nu/2}(kr)$	Boundary A φ_2 given by (75)	Boundary B $\varphi_2(r) = J_{\nu/2}(kr)$	N_1, N_2	N_3
16×16				9	21
32×32				9	28
64×64	5.1914	4.7202	4.132	17	34
128×128	1.7401	1.7984	3.536	24	40
256×256	4.2435	4.2284	4.1531	29	45
512×512	6.6806	6.6900	5.891	29	45
1024×1024	4.6762	4.6307	4.4284	29	45
2048×2048	3.7948	3.7857	3.8657	29	45

Consider the test problem

$$\Delta u + k^2 u = 0 \quad \text{on } \Omega, \tag{73a}$$

$$u\big|_{\Gamma_1} = \varphi_1(r) = 0, \quad u\big|_{\Gamma_2} = \varphi_2(r) = J_{\nu/2}(kr), \tag{73b}$$

$$u\big|_{\Gamma_3} = \varphi_3(\theta) = J_{\nu/2}(kr_3(\theta))\,\frac{\theta - \alpha}{2\pi - \alpha}, \tag{73c}$$

where Γ_3 may be Boundary A, B, C, or D. We can take v to be $v(r,\theta) = J_{\nu/2}(kr)\sin\left(\frac{\nu}{2}(\theta-\alpha)\right)$, since this function matches the boundary conditions on the sides of the wedge and satisfies the homogeneous Helmholtz equation. The derivatives of the Bessel function $J_{\nu/2}(kr)$ become unbounded as $r \to 0$, so there is an inhomogeneous contribution to the singularity from v. There is also a homogeneous contribution to the singularity from the Fourier–Bessel series, since $v(r,\theta)$ does not satisfy the boundary condition on Γ_3. To build the asymptotic series (9) for $v(r,\theta)$, we simply use several leading terms of the power series expansion for $J_{\nu/2}$, rather than apply the algorithm of Fox and Sankar [18]. The power series for the Bessel function of arbitrary order σ is

$$J_\sigma(x) = \sum_{l=0}^{\infty} \frac{(-1)^l}{l!\,\Gamma(l+\sigma+1)}\left(\frac{x}{2}\right)^{2l+\sigma}. \tag{74}$$

We use the convention that $v^{(m)}(r,\theta) = r^{(m-1)+\eta}(A_m(\theta)\ln r + B_m(\theta))$ with $\eta > 0$ (see equation (9)) so for $v(r,\theta) = J_{\nu/2}(kr)\sin\left(\frac{\nu}{2}(\theta-\alpha)\right)$ we take

$$v^{(2l+1)}(r,\theta) = \frac{(-1)^l}{l!\,\Gamma(l+\nu/2+1)}\left(\frac{kr}{2}\right)^{2l+\nu/2}\sin\left(\frac{\nu}{2}(\theta-\alpha)\right), \qquad v^{(2l+2)} = 0, \quad l = 0, 1, 2, \ldots.$$

The number of terms $v^{(m)}$ that must be included in the regularization depends on the required degree of regularity d. For our fourth order difference potentials formulation, $d = 4$ is sufficient. Then the inequalities (13) tell us that it is sufficient to include $M_v = 4$ terms of the asymptotic expansion (9) for v and $M_w = 7$ terms of the Fourier–Bessel series (7) in the regularization. In this case, the terms $v^{(m)}$ are 0 for even values of m, so the inhomogeneous portion of the regularization only contains 2 nonzero terms.

We utilize the SciPy function `odeint` for solving the initial value problems (43), with the absolute and relative tolerance set to 10^{-12}. The initial value problems are independent, but we solve all M_w of the ODEs with a single call to the numerical ODE integrator to reduce the number of Discrete Sine Transforms that must be performed. This performance consideration has been discussed in Section 2.4. Later in the regularization algorithm, when we form the linear system $W\boldsymbol{a} = p$ (see equation (53)) we take the dimension N_W of the discretization grid on Γ_3 to be 2048. The parameter M_a that determines the horizontal dimensional of matrix W also needs to be set. We have used $M_a = 200$ in our experiments, though a careful numerical study would be required to make more general recommendations about the value of M_a, since the optimal choice may depend on the shape and size of the boundary perturbation, among other factors. After obtaining the intensity factors, we create the regularized problem (57) and apply the method of difference potentials. On coarse grids, the method of difference potentials is fairly sensitive to the sizes of the Chebyshev basis sets. We determined appropriate sizes of the basis sets on coarse grids by testing many different choices for N_1, N_2, and N_3 under the constraint $N_1 = N_2$. Then, we chose the dimensions that minimized the difference between the numerical and expected solution for a smooth test problem with a known solution. On finer grids, the method is less sensitive to the basis dimensions, but highly oscillatory solutions naturally require a greater number of basis functions to achieve the desired accuracy. For each of our numerical experiments, we list the dimensions of the basis sets along with the convergence rates (see Tables 1 and 2).

The expected solution to test problem (73) cannot be computed with arbitrary accuracy since it requires the summation of an infinite Fourier–Bessel series. Thus, we cannot use the expected solution to measure the rate of convergence. Instead,

Table 2
Convergence results and the sizes of the basis sets for boundary value problem (76) with $k = 10.75$ and $\alpha = \pi/2$.

Grid	Convergence rate		Basis dimensions	
	Boundary C	Boundary D	N_1, N_2	N_3
16×16			5	25
32×32			20	30
64×64	9.7393	8.7996	30	40
128×128	1.1455	0.1715	40	55
256×256	4.0674	0.8651	60	70
512×512	5.8289	6.7732	60	90
1024×1024	4.5438	6.4244	60	110
2048×2048	4.0053	4.0219	60	110

we track the convergence by comparing the numerical solution on successive grids. If $u^{(N)}$ denotes the numerical solution on the $N \times N$ grid, then the convergence rate on the $N \times N$ grid is defined as

$$\log_2 \frac{\|u^{(N/2)} - u^{(N/4)}\|_\infty}{\|u^{(N)} - u^{(N/2)}\|_\infty}.$$

Table 1 shows the convergence results for test problem (73) on Boundaries A and B. The functions φ_1 and φ_2 are only defined for $r \in [0, R]$ and must be smoothly extended to the larger interval $[0, R_{\text{arc}}]$. In all cases we take $\varphi_1(r) = 0$ for all $r \in [0, R_{\text{arc}}]$, but we consider two different extensions for φ_2 to corroborate our claim that any sufficiently smooth extension will work. In the first and third columns of Table 1, we define $\varphi_2(r) = J_{\nu/2}(kr)$ for $r \in [0, R_{\text{arc}}]$, while in the second column we have defined

$$\varphi_2(r) = J_{\nu/2}(kr) + \begin{cases} 0, & \text{if } r \le R, \\ (r-R)^5, & \text{if } r > R, \end{cases} \qquad r \in [0, R_{\text{arc}}]. \tag{75}$$

Table 1 shows fourth order convergence regardless of the choice of extension.

Next, we consider a boundary value problem that has nonzero data on both sides of the wedge,

$$\Delta u + k^2 u = 0 \quad \text{on } \Omega, \tag{76a}$$

$$u\big|_{\Gamma_1} = \varphi_1(r) = J_{3\nu/2}(kr), \quad u\big|_{\Gamma_2} = \varphi_2(r) = J_{\nu/2}(kr), \tag{76b}$$

$$u\big|_{\Gamma_3} = \varphi_3(\theta) = J_{3\nu/2}(kr_3(\theta)) + \left[J_{\nu/2}(kr_3(\theta)) - J_{3\nu/2}(kr_3(\theta))\right] \cdot \frac{(\theta-\alpha)(\theta-(2\pi-\alpha))}{\alpha(2\pi-\alpha)}. \tag{76c}$$

This problem has been designed so that $v(r,\theta) = J_{\nu/2}(kr)\sin\left(\frac{\nu}{2}(\theta-\alpha)\right) + J_{3\nu/2}(kr)\sin\left(\frac{3\nu}{2}(\theta-\alpha)\right)$. The asymptotic series (9) for v is again built using the power series expansion (74) of the Bessel function,

$$v^{(2l+1)}(r,\theta) = \frac{(-1)^l\,(kr/2)^{2l+\nu/2}}{l!\,\Gamma(l+\nu/2+1)}\sin\left(\frac{\nu}{2}(\theta-\alpha)\right) + \frac{(-1)^l\,(kr/2)^{2l+3\nu/2}}{l!\,\Gamma(l+3\nu/2+1)}\sin\left(\frac{3\nu}{2}(\theta-\alpha)\right),$$
$$v^{(2l+2)} = 0, \qquad l = 0, 1, 2, \ldots.$$

The convergence results for test problem (76) are presented in Table 2 for the case $\alpha = \pi/2$, in which the corner is a right angle. Again, there is fourth order convergence as the grid is refined.

5. Conclusions

The solution to the two-dimensional Helmholtz equation typically becomes singular in the neighborhood of a reentrant corner in the domain. We designed an algorithm that determines the form of the singularity and subtracts it to produce a regularized problem. The outer boundary of the computational domain is allowed to take on a general smooth shape, so we employ the method of difference potentials to solve the regularized problem with high-order accuracy. The method of difference potentials uses finite difference schemes to obtain an efficient and accurate approximation, even on general geometries that do not conform to the grid. The formulation of the method of difference potentials presented here is equivalent to formulations of the method for smooth boundaries, except that we take independent basis sets on each segment of the boundary and have modified the standard equation-based extension near the corners.

Computing the regularization is challenging because the singularity may have both a local, inhomogeneous contribution due to the boundary data on the sides of the wedge, and a nonlocal, homogeneous contribution from singular solutions that are zero on the sides of the wedge. Our algorithm removes the inhomogeneous contribution by utilizing the method of Fox and Sankar [18] to build an asymptotic series solution in the neighborhood of the corner. The homogeneous contribution

to the singularity is nonlocal because the intensity factors which characterize it are determined by the boundary condition on the outer boundary, far from the corner. To obtain the unknown intensity factors, we use separation of variables and an intermediate finite difference problem to reduce the original boundary value problem to one with homogeneous boundary conditions on the wedge. Then we obtain the intensity factors by formulating an overdetermined linear system at the outer boundary.

This work is significant because to the best of our knowledge it is the first time that the Helmholtz equation has been solved near a reentrant corner when both the homogeneous and inhomogeneous contributions to the singularity are present. Another advantage of our method over other work published in the literature is that the regularization is computed with sufficient accuracy to guarantee an overall high-order of accuracy, as confirmed by our numerical experiments. Together with our previous work [31,32,10,33], this paper shows that difference potentials is a flexible and robust numerical method for the Helmholtz equation, capable of handling nonstandard boundary conditions, multiple scattering, and singularities due to both geometric irregularities and discontinuous data. Moreover, the approach to regularization presented in Section 2 can be used with other numerical methods, not only the method of difference potentials.

Future work could extend the methodology presented in this paper to more difficult cases, such as reentrant corners with other types of boundary conditions (beyond Dirichlet), reentrant corners that lie on the interface between two materials, or time-dependent waves. In particular, it should be relatively straightforward to handle Neumann boundary conditions at the wedge, or the mixed case in which there is a Dirichlet boundary conditions on one side of the wedge and a Neumann boundary condition on its other side. Indeed, the corresponding expansions for the inhomogeneous contribution to singularity are already given by Fox and Sankar [18], and the Fourier–Bessel expansions for the homogeneous part can also be constructed. Other types of boundary conditions on the sides of the wedge, including Robin and those that characterize material interfaces, can also be accommodated, but it is likely to require additional work. As far as the remote boundary Γ_3, boundary conditions other than the Dirichlet boundary condition can be set there similarly to how it is done in the general implementations of the method of difference potentials, see, e.g. [10].

The main challenge in having the current work extended to the case of three space dimensions is that unlike in 2D where the only kind of boundary irregularity is a corner, the 3D geometry offers a much broader variety of the possible boundary irregularities. For example, a polyhedron may have both reentrant edges, i.e., dihedral angles, and vertices, i.e., polyhedral angles. For the latter, the number of facets may vary from one vertex to another. We expect that our 2D regularization methodology described in Section 2 may extend to dihedral angles in 3D with relatively little additional effort, at least for those locations on the edge that are away from its endpoints. Developing the regularizing expansions for polyhedral reentrant angles may, on the other hand, prove a major undertaking. Moreover, the 3D shapes are obviously not limited to polyhedra, and there may be more general reentrant solid angles, e.g., conical. For some of those solid angles there may be separation of variables and hence a way of building a regularizing expansion.

Acknowledgement

We would like to thank the referee of the paper for her/his helpful comments and suggestions.

References

[1] J.E. Akin, The generation of elements with singularities, Int. J. Numer. Methods Eng. 10 (6) (1976) 1249–1259, http://dx.doi.org/10.1002/nme.1620100605.
[2] P. Amore, Solving the Helmholtz equation for membranes of arbitrary shape: numerical results, J. Phys. A 41 (26) (2008) 265206, http://dx.doi.org/10.1088/1751-8113/41/26/265206.
[3] I.M. Babuška, S.A. Sauter, Is the pollution effect of the FEM avoidable for the Helmholtz equation considering high wave numbers?, SIAM Rev. 42 (3) (2000) 451–484 (electronic), reprint of SIAM J. Numer. Anal. 34 (6) (1997) 2392–2423, MR1480387 (99b:65135).
[4] K.-J. Bathe, E.L. Wilson, Numerical Methods in Finite Element Analysis, Prentice-Hall, Englewood Cliffs, NJ, 1976.
[5] A. Bayliss, C.I. Goldstein, E. Turkel, On accuracy conditions for the numerical computation of waves, J. Comput. Phys. 59 (3) (1985) 396–404.
[6] T. Betcke, L.N. Trefethen, Reviving the method of particular solutions, SIAM Rev. 47 (3) (2005) 469–491, http://dx.doi.org/10.1137/S0036144503437336 (electronic).
[7] T.L. Binford Jr., D.P. Nicholls, N. Nigam, T. Warburton, Exact non-reflecting boundary conditions on perturbed domains and *hp*-finite elements, J. Sci. Comput. 39 (2) (2009) 265–292, http://dx.doi.org/10.1007/s10915-008-9263-z.
[8] S. Britt, S. Tsynkov, E. Turkel, A compact fourth order scheme for the Helmholtz equation in polar coordinates, J. Sci. Comput. 45 (1–3) (2010) 26–47, http://dx.doi.org/10.1007/s10915-010-9348-3.
[9] S. Britt, S. Tsynkov, E. Turkel, Numerical simulation of time-harmonic waves in inhomogeneous media using compact high order schemes, Commun. Comput. Phys. 9 (3) (2011) 520–541, http://dx.doi.org/10.4208/cicp.091209.080410s.
[10] D.S. Britt, S.V. Tsynkov, E. Turkel, A high-order numerical method for the Helmholtz equation with nonstandard boundary conditions, SIAM J. Sci. Comput. 35 (5) (2013) A2255–A2292, http://dx.doi.org/10.1137/120902689.
[11] S. Britt, S. Petropavlovsky, S. Tsynkov, E. Turkel, Computation of singular solutions to the Helmholtz equation with high order accuracy, Appl. Numer. Math. 93 (2015) 215–241, http://dx.doi.org/10.1016/j.apnum.2014.10.006.
[12] O.P. Bruno, T. Elling, A. Sen, A Fourier continuation method for the solution of elliptic eigenvalue problems in general domains, Math. Probl. Eng. (2015) 184786, http://dx.doi.org/10.1155/2015/184786.
[13] L. Chindelevitch, D.P. Nicholls, N. Nigam, Error analysis and preconditioning for an enhanced DtN-FE algorithm for exterior scattering problems, J. Comput. Appl. Math. 204 (2) (2007) 493–504, http://dx.doi.org/10.1016/j.cam.2006.02.051.
[14] J.B. Conway, A Course in Functional Analysis, 2nd edition, Grad. Texts Math., vol. 96, Springer-Verlag, New York, 1990.
[15] A. Deraemaeker, I.M. Babuška, P. Bouillard, Dispersion and pollution of the FEM solution for the Helmholtz equation in one, two and three dimensions, Int. J. Numer. Methods Eng. 46 (1999) 471–499.

[16] C. Farhat, I. Harari, L. Franca, The discontinuous enrichment method, Comput. Methods Appl. Mech. Eng. 190 (2001) 6455–6479.
[17] C. Farhat, R. Tezaur, J. Toivanen, A domain decomposition method for discontinuous Galerkin discretizations of Helmholtz problems with plane waves and Lagrange multipliers, Int. J. Numer. Methods Eng. 78 (13) (2009) 1513–1531, http://dx.doi.org/10.1002/nme.2534.
[18] L. Fox, R. Sankar, Boundary singularities in linear elliptic differential equations, J. Inst. Math. Appl. 5 (1969) 340–350.
[19] I.C. Gohberg, M.G. Kreĭn, Introduction to the theory of linear nonselfadjoint operators, Translated from Russian by A. Feinstein, Transl. Math. Monogr., vol. 18, American Mathematical Society, Providence, RI, 1969.
[20] I. Harari, E. Turkel, Accurate finite difference methods for time-harmonic wave propagation, J. Comput. Phys. 119 (2) (1995) 252–270.
[21] J. Helsing, A. Jonsson, On the computation of stress fields on polygonal domains with V-notches, Int. J. Numer. Methods Eng. 53 (2) (2002) 433–453, http://dx.doi.org/10.1002/nme.291.
[22] J.S. Hesthaven, T. Warburton, Nodal Discontinuous Galerkin Methods: Algorithms, Analysis, and Applications, Texts Appl. Math., vol. 54, Springer, New York, 2008.
[23] C. Huang, Z. Wu, R.D. Nevels, Edge diffraction in the vicinity of the tip of a composite wedge, IEEE Trans. Geosci. Remote Sens. 31 (5) (1993) 1044–1050, http://dx.doi.org/10.1109/36.263775.
[24] D.S. Kamenetskii, A Numerical Method for Solving a Singular Boundary Value Problem for the Chaplygin Equation in the Hodograph Plane, Preprint 60, Keldysh Institute for Applied Mathematics, Russian Academy of Sciences, Moscow, Russia, 1992, in Russian.
[25] D.S. Kamenetskii, V.S. Ryaben'kii, Solution of Boundary Value Problems for the Laplace Equation in a Domain with a Cut by the Method of Difference Potentials, Preprint 33, Keldysh Institute for Applied Mathematics, USSR Academy of Sciences, Moscow, USSR, 1990, in Russian.
[26] D.S. Kamenetskii, E.G. Shifrin, Design of Nozzle Blades of a Gas Turbine by the Method of Hodograph, Preprint 61, Keldysh Institute for Applied Mathematics, Russian Academy of Sciences, Moscow, Russia, 1992, in Russian.
[27] V. Mantič, F. París, J. Berger, Singularities in 2D anisotropic potential problems in multi-material corners: real variable approach, Int. J. Solids Struct. 40 (20) (2003) 5197–5218, http://dx.doi.org/10.1016/S0020-7683(03)00292-0.
[28] L. Marin, Treatment of singularities in the method of fundamental solutions for two-dimensional Helmholtz-type equations, Appl. Math. Model. 34 (6) (2010) 1615–1633, http://dx.doi.org/10.1016/j.apm.2009.09.009.
[29] L. Marin, D. Lesnic, V. Mantič, Treatment of singularities in Helmholtz-type equations using the boundary element method, J. Sound Vib. 278 (1–2) (2004) 39–62, http://dx.doi.org/10.1016/j.jsv.2003.09.059.
[30] P.G. Martinsson, A direct solver for variable coefficient elliptic PDEs discretized via a composite spectral collocation method, J. Comput. Phys. 242 (2013) 460–479, http://dx.doi.org/10.1016/j.jcp.2013.02.019.
[31] M. Medvinsky, S. Tsynkov, E. Turkel, The method of difference potentials for the Helmholtz equation using compact high order schemes, J. Sci. Comput. 53 (1) (2012) 150–193, http://dx.doi.org/10.1007/s10915-012-9602-y.
[32] M. Medvinsky, S. Tsynkov, E. Turkel, High order numerical simulation of the transmission and scattering of waves using the method of difference potentials, J. Comput. Phys. 243 (2013) 305–322, http://dx.doi.org/10.1016/j.jcp.2013.03.014.
[33] M. Medvinsky, S. Tsynkov, E. Turkel, Solving the Helmholtz equation for general smooth geometry using simple grids, Wave Motion 62 (2016) 75–97, http://dx.doi.org/10.1016/j.wavemoti.2015.12.004.
[34] D.P. Nicholls, N. Nigam, Exact non-reflecting boundary conditions on general domains, J. Comput. Phys. 194 (1) (2004) 278–303, http://dx.doi.org/10.1016/j.jcp.2003.09.006.
[35] D.P. Nicholls, N. Nigam, Error analysis of an enhanced DtN-FE method for exterior scattering problems, Numer. Math. 105 (2) (2006) 267–298, http://dx.doi.org/10.1007/s00211-006-0040-3.
[36] A.A. Reznik, Approximation of surface potentials of elliptic operators by difference potentials, Dokl. Akad. Nauk SSSR 263 (6) (1982) 1318–1321.
[37] V.S. Ryaben'kii, Boundary equations with projections, Russ. Math. Surv. 40 (2) (1985) 147–183.
[38] V.S. Ryaben'kii, Method of Difference Potentials and Its Applications, Springer Ser. Comput. Math., vol. 30, Springer-Verlag, Berlin, 2002.
[39] V.S. Ryaben'kii, S.V. Utyuzhnikov, An algorithm of the method of difference potentials for domains with cuts, Appl. Numer. Math. 93 (2015) 254–261, http://dx.doi.org/10.1016/j.apnum.2014.02.007.
[40] I. Singer, E. Turkel, High-order finite difference methods for the Helmholtz equation, Comput. Methods Appl. Mech. Eng. 163 (1–4) (1998) 343–358.
[41] I. Singer, E. Turkel, Sixth-order accurate finite difference schemes for the Helmholtz equation, J. Comput. Acoust. 14 (3) (2006) 339–351, http://dx.doi.org/10.1142/S0218396X06003050.
[42] G.E. Sneddon, W.W. Read, The method of particular solutions for the Helmholtz equation, ANZIAM J. 46 (C) (2004/2005) C544–C557.
[43] R.W. Thatcher, The use of infinite grid refinements at singularities in the solution of Laplace's equation, Numer. Math. 25 (2) (1975/76) 163–178.
[44] S.V. Tsynkov, On the definition of surface potentials for finite-difference operators, J. Sci. Comput. 18 (2) (2003) 155–189, http://dx.doi.org/10.1023/A:1021111713715.
[45] E. Turkel, D. Gordon, R. Gordon, S. Tsynkov, Compact 2D and 3D sixth order schemes for the Helmholtz equation with variable wave number, J. Comput. Phys. 232 (1) (2013) 272–287, http://dx.doi.org/10.1016/j.jcp.2012.08.016.
[46] D. Wang, R. Tezaur, J. Toivanen, C. Farhat, Overview of the discontinuous enrichment method, the ultra-weak variational formulation, and the partition of unity method for acoustic scattering in the medium frequency regime and performance comparisons, Int. J. Numer. Methods Eng. 89 (4) (2012) 403–417, http://dx.doi.org/10.1002/nme.3239.
[47] W.H. Woodward, S. Utyuzhnikov, P. Massin, On the application of the method of difference potentials to linear elastic fracture mechanics, Int. J. Numer. Methods Eng. 103 (10) (2015) 703–736, http://dx.doi.org/10.1002/nme.4903.
[48] W.H. Woodward, S. Utyuzhnikov, P. Massin, Developments on the method of difference potentials for linear elastic fracture mechanics problems, Int. J. Numer. Methods Eng. (2017), submitted for publication.